Inorganic Chemistry
Cite This: Inorg. Chem. 2018, 57, 6362−6375
Article
pubs.acs.org/IC

Designing a Dy_2 Single-Molecule Magnet with Two Well-Differentiated Relaxation Processes by Using a Nonsymmetric Bis-bidentate Bipyrimidine-*N*-Oxide Ligand: A Comparison with Mononuclear Counterparts

Ismael F. Díaz-Ortega,[†] Juan Manuel Herrera,[*,†] Daniel Aravena,[‡] Eliseo Ruiz,[§] Tulika Gupta,[#] Gopalan Rajaraman,[*,#] H. Nojiri,[*,¶] and Enrique Colacio[*,†]

[†]Departamento de Química Inorgánica, Facultad de Ciencias, Universidad de Granada, Avenida Fuentenueva s/n, 18071 Granada, Spain

[‡]Departamento de Química de los Materiales, Facultad de Química y Biología, Universidad de Santiago de Chile, Casilla 40, Correo 33, Santiago, Chile

[§]Departament de Química Inorgànica and Institut de Recerca de Química Teòrica i Computacional, Universitat de Barcelona, Diagonal 645, 08028 Barcelona, Spain

[#]Department of Chemistry, Indian Institute of Technology Bombay, Powai, Mumbai 400076, India

[¶]Institute for Materials Research, Tohoku University, Katahira, Sendai, 980-8577, Japan

Supporting Information

ABSTRACT: Herein we report a dinuclear [(μ-mbpymNO)-{$(tmh)_3Dy$}$_2$] (**1**) single-molecule magnet (SMM) showing two nonequivalent Dy^{III} centers, which was rationally prepared from the reaction of $Dy(tmh)_3$ moieties (tmh = 2,2,6,6-tetramethyl-3,5-heptanedionate) and the asymmetric bis-bidentate bridging ligand 4-methylbipyrimidine (mbpymNO). Depending on whether the Dy^{III} ions coordinate to the N^O or N^N bidentate donor sets, the Dy^{III} sites present a NO_7 (D_{2d} geometry) or N_2O_6 (D_{4d}) coordination sphere. As a consequence, two different thermally activated magnetic relaxation processes are observed with anisotropy barriers of 47.8 and 54.7 K. Ab initio calculations confirm the existence of two different relaxation phenomena and allow one to assign the 47.8 and 54.7 K energy barriers to the $Dy(N_2O_6)$ and $Dy(NO_7)$ sites, respectively. Two mononuclear complexes, [$Dy(tta)_3$(mbpymNO)] (**2**) and [$Dy(tmh)_3$(phenNO)] (**3**), have also been prepared for comparative purposes. In both cases, the Dy^{III} center shows a NO_7 coordination sphere and SMM behavior is observed with U_{eff} values of 71.5 K (**2**) and 120.7 K (**3**). In all three cases, ab initio calculations indicate that relaxation of the magnetization takes place mainly via the first excited-state Kramers doublet through Orbach, Raman, and thermally assisted quantum-tunnelling mechanisms. Pulse magnetization measurements reveal that the dinuclear and mononuclear complexes exhibit hysteresis loops with double- and single-step structures, respectively, thus supporting their SMM behavior.

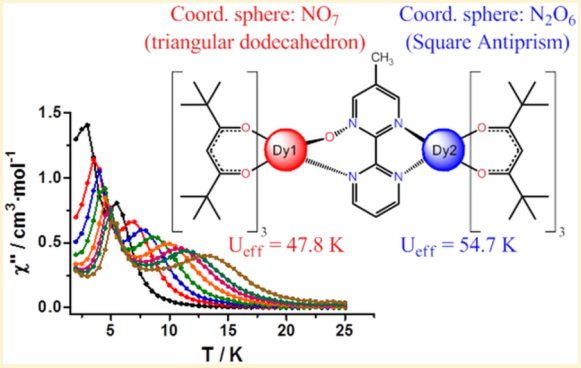

INTRODUCTION

The study of molecular magnetic systems has undergone an extraordinary development over the last 3 decades because of the finding that some coordination compounds exhibit magnetization blocking and a hysteresis loop below a critical temperature T_B (blocking temperature).[1] These molecules, called single-molecule magnets (SMMs), could find applications in the emerging fields of quantum computing, molecular spintronics, and ultrahigh-density magnetic recording.[2−5] These systems owe their behavior to the existence of an energy barrier that avoids magnetic relaxation when the magnetic field is canceled. The larger the energy barrier height, the larger T_B should be; however, the existence of fast magnetic relaxation through quantum tunnelling can dramatically reduce T_B.

The research activity in the field of SMMs has been mainly focused along four lines: (i) Synthesis of novel members of this family. (ii) Study of the structural and electronic factors governing the SMM behavior. In this regard, feedback between the experiment and theory has been crucial for the successful development of this line of research. (iii) Deliberate design of SMMs with increasing T_B (temperature at which the magnetic hysteresis opens at zero field for a definite sweep rate) by

Received: February 15, 2018
Published: May 18, 2018

DOI: 10.1021/acs.inorgchem.8b00427
Inorg. Chem. 2018, 57, 6362−6375

making use of suitable strategies based on the new generated knowledge. (iv) Incorporation of SMMs in nanosized devices. Progress made in research lines (i)−(iii) has allowed the preparation of SMMs with U and T_B values as high as 1837 and 60 K, respectively.[6] These achievements have been mainly reached with high axially symmetric Dy^{3+} complexes because (i) Dy^{3+} is a Kramers ion with a doubly degenerate $\pm m_j$ ground state, for which quantum tunnelling relaxation of the magnetization (QTM) should be forbidden in the absence of a magnetic field (QTM usually prevents the observation of magnetic hysteresis at zero magnetic field in lanthanide complexes).[1b] (ii) It has a large magnetic moment in the ground state, and (iii) the anisotropic oblate-shaped f electron density of the Dy^{III} ion requires an appropriate axial crystal field to induce axial magnetic anisotropy in the ground state.[1b] The larger the axial magnetic anisotropy (complex with ideal axial symmetry and shorter Dy^{III}-donor bond distances involving axial positions), the smaller the QTM and the larger T_B.

Slow relaxation of the magnetization passing from a magnet state to a paramagnetic state in Dy^{III} SMMs is a very intricate process that can take place through the ground and the first and/or even higher low-lying excited states, generally via multiple processes (QTM, one-phonon direct, two-phonon Raman and Orbach, etc.).[1] It is worth noting that, for some SMMs, two thermally activated processes of molecular origin have been observed, even in mononuclear and polynuclear complexes with crystallographically equivalent Dy^{III} ions.[7] Moreover, in a few cases, it has been demonstrated by magnetic dilution studies that one of these processes is really intermolecular in origin.[8] Regardless of the origin of the relaxation processes (molecular with equivalent or nonequivalent Dy^{III} ions or intermolecular), their presence was generally a matter of serendipity because the ligand was not deliberately designed to afford two nonequivalent Dy^{III} sites. In view of this, we decided to design a new neutral bis-bidentate bridging ligand, 4-methylbipyrimidine-2-*N*-oxide (mbpymNO) with two different bidentate donor sets and chelating rings (six-membered NO and five-membered N_2), which, when acting in a bis-bidentate coordination mode, will mandatorily afford Dy^{III} complexes with two different Dy^{III} coordination spheres. Although over the past few years pyridine-*N*-oxide derivatives have been used as ligands to prepare Dy^{III}-containing SMMs, the number of reported examples is still limited.[9] The present paper reports the synthesis, crystal structure, detailed alternating-current (ac) and direct-current (dc) magnetic studies, and ab initio theoretical calculations of the dinuclear complex $[(\mu\text{-mbpymNO})\{(tmh)_3Dy\}_2]$ (**1**) as well as of the mononuclear complexes $[Dy(tta)_3(mbpymNO)]$ (**2**) and $[Dy(tmh)_3(phenNO)]$ (**3**) for comparative purposes. On the basis of previous results with diazine and tetrazine complexes containing β-diketonato ancillary ligands,[10] the reported complexes are expected to exhibit SMM behavior. The aim of this study is 4-fold: (i) to confirm the existence of two well-differentiated thermally activated processes, (ii) to prove the single-ion origin of these relaxation processes, (iii) to assign each relaxation processes to each type of Dy^{III} coordination sphere, and (iv) to draw useful conclusions for future development of the field.

EXPERIMENTAL SECTION

General Procedures. 1,10-Phenanthroline-1-oxide (phenNO) was prepared according to the reported procedure described by Corey et al.[11] The ligands 2,2,6,6-tetramethyl-3,5-heptanedione (Htmh), 2-thenoyltrifluoroacetone (Htta), solvents, and dysprosium salts were purchased from commercial sources and used as received.

Synthesis of the Ligand 4-Methyl-2,2′-bipyrimidine-2-oxide (mbpymNO). This ligand was prepared in two steps, as shown in Scheme 1. First, 2-cyanopyrimidine (0.02 mol, 2.1 g), hydroxylamine hydrochloride (0.04 mol, 2.8 g), and sodium hydrogen carbonate (0.04 mol, 3.36 g) were dissolved in water (40 mL) and stirred vigorously at room temperature. After 1 h, a white precipitate corresponding to the intermediate product (*E*)-*N*′-hydroxypyrimidine-2-carboximidamide appeared.[12] The solid was filtered, washed with water, dried under vacuum, and used in the next step without any further purification. In a second step, 0.018 mol of (*E*)-*N*′-hydroxypyrimidine-2-carboximidamide was mixed with equimolar amounts of 3-ethoxy-2-methylpropenal and trifluoroacetic acid in 25 mL of 2-propanol, and the resulting solution was heated at 80 °C for 12 h. After this time, the resulting mbpymNO ligand precipitated as a white powder, which was filtered, washed with ethanol, and dried under vacuum. Yield: 76%. Anal. Calcd (found) for $C_9H_8N_4O$: C, 57.42 (55.05); H, 4.28 (4.54); N, 29.78 (30.50). ^{1}H NMR (400 MHz, DMSO-d^6): δ 8.99 (d, J = 4.96 Hz, 2H), 8.69 (s, 1H), 8.29 (s, 1H), 7.66 (t, J = 4.92 Hz, 1H), 2.33 (s, 3H). MS (ESI). Calcd (found) for $C_9H_9N_4O^+$: m/z 189.08 (189.0777).

Scheme 1. Synthesis of the mbpymNO Ligand

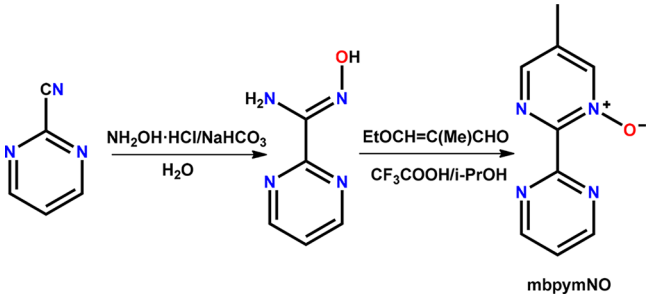

Synthesis of Complexes. *[{Dy(tmh)$_3$}$_2$(μ_2-mbpymNO)]·MeOH (**1**).* A total of 0.375 mmol (0.170 g) of $Dy(NO_3)_3\cdot 6H_2O$ dissolved in methanol (5 mL) was added to a solution of Htmh (1.125 mmol, 235 μL) and Et_3N (1.125 mmol, 156 μL) in methanol (5 mL). The solution was stirred for 10 min and then added dropwise to a solution of mbpymNO (0.187 mmol, 0.035 g) dissolved in 5 mL of methanol. The resulting solution was allowed to stand at room temperature. Partial evaporation of the solvent afforded a good crop of **1** as single crystals, which were filtered, washed with a minimum amount of ethanol, and air-dried. Yield: 166 mg (53.8%). Anal. Calcd for $C_{75}H_{122}N_4O_{13}Dy_2\cdot CH_3OH$: C, 55.49; H, 7.72; N, 3.41. Found: C, 56.20; H, 7.80; N, 3.21.

*[Dy(tta)$_3$(mbpymNO)] (**2**).* This complex was prepared as **1** but using Htta instead of Htmh and a molar ratio $[Dy(tmh)_3]$/mbpymNO of 1:1. Yield: 90 mg (47.5%). Anal. Calcd for $C_{33}H_{20}N_4O_7F_9S_3Dy$ (**1**): C, 39.10; H, 1.99; N, 5.52. Found: C, 40.03; H, 2.23; N, 5.30.

*[Dy(tmh)$_3$(phenNO)] (**3**).* This complex was prepared as **2** but using the ligand Htmh instead of Htta and phenNO instead of mbpymNO. Yield: 110 mg (65%). Anal. Calcd for $C_{45}H_{65}N_2O_7Dy$ (**3**): C, 59.49; H, 7.21; N, 3.1. Found: C, 58.67; H, 7.68; N, 3.32.

X-ray Crystallography. Suitable crystals of complexes **1**−**3** were mounted on a Bruker D8 Venture diffractometer (Mo Kα radiation, λ = 0.71073 Å, Photon 100 CMOS detector). Details of the crystals, data collection, and refinement parameters are reported in Table S1. Once the data were processed (raw data integration, merging of equivalent reflections, and empirical correction of the absorption), the structures were solved by either Patterson or direct methods and refined by full-matrix least squares on weighted F^2 values using the *SHELX* suite of programs[13] integrated in *Olex2*.[14] Selected bond lengths and angles can also be found in Tables S2−S4. CCDC 1540135 (**1**), 1540134 (**2**), and 1540133 (**3**) contain the supplementary crystallographic data for this paper. These data are provided free of charge by the Cambridge Crystallographic Data Centre.

DOI: 10.1021/acs.inorgchem.8b00427
Inorg. Chem. 2018, 57, 6362−6375

Scheme 2. Syntheses of Complexes 1 and 2 (a) and 3 (b)

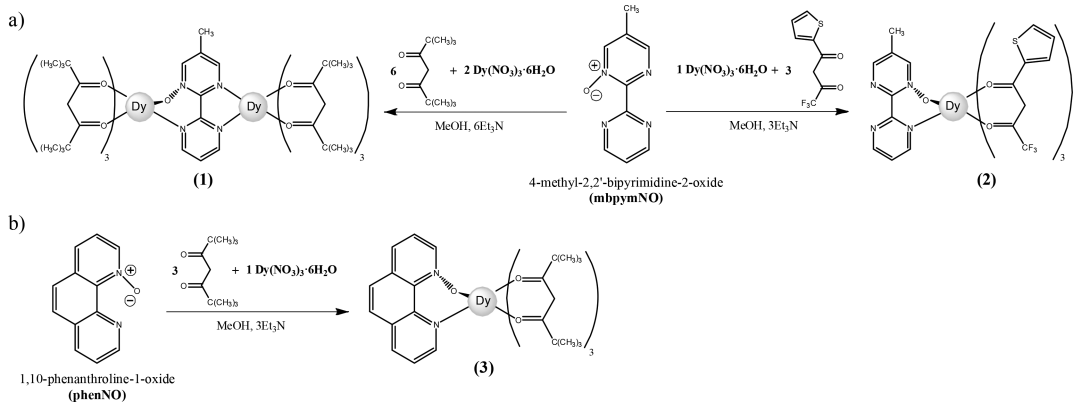

Physical Measurements. Elemental analyses were carried out at the "Centro de Instrumentación Científica" of the University of Granada on a Fisons-Carlo Erba analyzer model EA 1108. Fourier tranform infrared (FT-IR) spectra were recorded with a Bruker Tensor 27 spectrometer using an ATR accessory. dc and ac susceptibility measurements were performed with a Quantum Design SQUID MPMS XL-5 device. ac experiments were performed using an oscillating ac field of 3.5 Oe and frequencies ranging from 1 to 1500 Hz. ac magnetic susceptibility measurements in the range 1−10000 Hz were carried out with a Quantum Design Physical Property Measurement System using an oscillating ac field of 5 Oe. Low-temperature magnetization measurements were performed by means of a conventional inductive probe in pulsed magnetic fields. The temperature reached as low as 0.4 K using a ^{3}He cryostat.[15] Polycrystalline specimens were mounted in a capillary tube made of polyimide. Samples of approximately 20 mg were not fixed within the sample tube, and then they aligned along the magnetic field direction. Subsequently, a magnetic field was applied several times until the orientation effect was saturated and the magnetization curves obtained in further shots were found to be identical.

Computational Methodology. The *MOLCAS 8.0* program package[16] was used to perform post-Hartree−Fock ab initio calculations. Using a multiconfigurational approach, relativistic effects were treated in two steps, based on Douglas−Kroll Hamiltonian. For the generation of basis sets, scalar terms were included, which were used to determine spin-free wave functions and also energies through the use of the complete-active space self-consistent-field (CASSCF) method.[17] Thus, spin−orbit free states were obtained by employing the RASSCF method, whereas spin−orbit coupling was taken into account using the RASSI-SO method,[18] which uses CASSCF wave functions as the basis sets and multiconfigurational wave functions as input states. The resulting wave functions and the energies of the molecular multiplets were used for calculation of the magnetic properties and **g** tensors of the lowest state using a specially designed routine *SINGLE_ANISO*.[19] As a consequence, the magnetic properties of a single magnetic ion are calculated by a fully ab initio approach in which the spin−orbit coupling is considered nonperturbatively. The active space in the CASSCF calculations comprised 9 electrons in 7 orbitals for the Dy^{III} ion, with a [ANO-RCC···9s8p6d4f3g2h] basis set for Dy^{III}, [ANO-RCC···4s3p1d] for N and O, [ANO-RCC···4s3p1d] for S, [ANO-RCC···3s2p] for C and F, and [ANO-RCC···2s] for H. A total of 21 sextets, 224 quadruplets, and 158 triplets were computed, while in RASSI, we had mixed 21 sextets, 128 quadruplets, and 98 doublets. For complex **1**, an additional approach was considered (approach II) with basis sets [ANO-RCC···7s6p4d2f] for Dy^{III}, [ANO-RCC···3s2p] for N and O, [ANO-RCC···4s3p] for S, [ANO-RCC···3s2p] for C and F, and [ANO-RCC···2s] for H. Calculations with approach II were executed at the ground state (S = 6) with 21 configurations (sextets). All of the ANO-RCC basis sets were adopted from the MOLCAS ANO-RCC library.[16b] In order to save disk space, Cholesky decomposition possessing a threshold of 0.2×10^{-7} was incorporated for our calculations.[20] Magnetic exchange interactions, exchange spectra, and all other magnetic properties of the Dy_2 dinuclear complex were deduced within the *POLY_ANISO*[21] routine based on the ab initio results of individual metal fragments.[22]

RESULTS AND DISCUSSION

Syntheses and Crystal Structures. Single crystals of the dinuclear complex **1** appeared after partial evaporation of a methanolic solution containing a mixture of $Dy(NO_3)_3{\cdot}6H_2O$, triethylamine, the β-diketone ligand Htmh, and the *N*-oxide ligand mbpymNO in a molar ratio of 1:3:3:0.5. The mononuclear complexes **2** and **3** were obtained following a similar procedure from the respective β-diketone (Htta for **2** and Htmh for **3**) and the *N*-oxide ligands (mbpymNO for **2** and phenNO for **3**), but in these cases, the molar ratio of the reactants was 1:3:3:1 (Scheme 2). Efforts to prepare the dinuclear $[\{Dy(tta)_3\}_2(\mu_2\text{-mbpymNO})]$ analogue were unsuccessful, and only the mononuclear complex was obtained. Queerly, we were also unable to isolate the mononuclear $[\{Dy(tmh)_3\}_2(\mu_1\text{-mbpymNO})]$ complex, and all of the essays performed led to the dinuclear specimen, regardless of the Dy/mbpymNO stoichiometric ratio used in the reaction.

The dinuclear complex **1** crystallizes in the monoclinic $P2_1/c$ space group, and the structure consists of two $[Dy(tmh)_3]$ moieties connected through the nonsymmetric bis-bidentate mbpymNO ligand. Thus, the Dy^{III} centers show different coordination spheres. Whereas the ion Dy1 is coordinated to the mbpymNO ligand through the N^O bidentate site (NO_7 coordination sphere), the Dy2 center is coordinated to the opposed N^N site (N_2O_6 coordination sphere) (Figure 1a). Analysis of the eight-coordinated geometries around the Dy centers by the continuous-shape-measures (CShMs) method[23] reveals that Dy1 and Dy2 show coordination spheres that are intermediate between several ideal geometries, with the lowest CShMs parameters for the D_{2d} triangular dodecahedron (1.161) and D_{4d} square antiprism (0.805), respectively (Table S5). The Dy−O_{tmh} bond distances in both centers fall between 2.2754 Å (Dy1−O2) and 2.3556 Å (Dy1−O6), as expected for these kinds of complexes. The Dy1−$O_{mbpymNO}$ bond distance is also similar (2.3725 Å) and much shorter than the Dy−$N_{mbpymNO}$ distances, which are found in the range between 2.6080 and 2.6462 Å. The average Dy−O distances in the Dy2 atom are slightly shorter than those in Dy1 (2.30 and 2.32 Å, respectively). The pyrimidine rings in the mbpymNO ligand are mutually twisted at an angle of 17.33° (Figure S1), and the Dy1−O1−N1 angle deviates significantly from linearity with a value of 127.23(3)°. Within the molecule, the Dy1−Dy2

DOI: 10.1021/acs.inorgchem.8b00427
Inorg. Chem. 2018, 57, 6362−6375

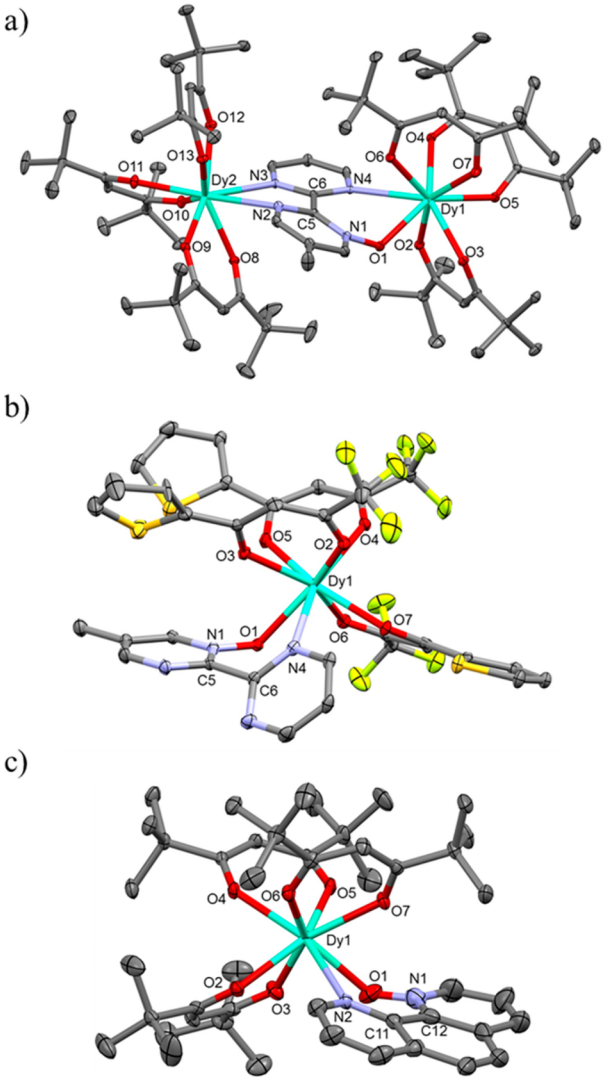

Figure 1. Crystal structures of complexes **1** (a), **2** (b). and **3** (c). Lattice solvents as well as H and disordered atoms have been omitted for the sake of clarity. Ellipsoids are drawn at 50% probability.

distance through the mbpymNO ligand is 7.099 Å. The shortest intermolecular distance between the Dy centers is 12.454 Å.

Regarding the mononuclear complexes **2** and **3**, they crystallize in space groups *Pbcn* (orthorhombic) and $P\bar{1}$ (triclinic), respectively. For **2**, the structure consists of mononuclear $[Dy(tta)_3(mbpymNO)]$ entities, where the Dy^{III} center exhibits a NO_7 coordination sphere with one N atom and one O atom belonging to the mbpymNO ligand and the six other O atoms to three deprotonated tta ligands (Figure 1b). The $Dy-O_{tta}$ bond distances are in the range 2.303(4)−2.361(3) Å, quite similar to the $Dy-O_{mbpymNO}$ distance of 2.317(4) Å and significantly shorter than the $Dy-N_{mbpymNO}$ bond distance of about 2.6 Å (selected bond distances and angles are reported in Table S3). For **3**, despite the replacement of ligands mbpymNO and tta by phenNO and tmh, respectively, the structure is quite similar to that of **2** (Figure 1c). The NO_7 coordination environment around the Dy^{III} center shows Dy−O and Dy−N bond distances that are in the same range as that observed for **2** (Table S4). Analysis of the coordination spheres around the Dy centers by the CShMs method (Table S5) reveals that in both cases the geometry is close to square-antiprismatic polyhedron (SAPR). Nevertheless, for **2**, the CShMs deviation parameter from an ideal SAPR (0.791) is slightly higher than that shown by **3** (0.566). It should be noted that the mononuclear complexes $[Dy(tta)_3(phen)]$ (phen = 1,10-phenanthroline) and $[Dy(tta)_3(bipy)]$ (bipy = 2,2′-bipyridine) show almost identical CShMs values between them (0.546 and 0.555) and with compound **3**, despite the different bidentate N,N or N,O and *β*-diketonate ligands.[24] In spite of the small bite of the bidentate N-oxide ligand [angle O1−Dy1−N4 = 67.60(13)° (**2**); angle O1−Dy1−N2 = 65.06(12)° (**3**)] compared to those exhibited by the *β*-diketonate ligands [in the ranges between 72.22(12)° for O6−Dy1−O7 and 73.12(13)° for O2−Dy1−O3 for **2** and 71.67(10)° for O2−Dy1−O3 and 73.27(9)° for O4−Dy1−O5 for **3**], the NO_7 coordination spheres are not seriously distorted from SAPR. The structural features involving the *N*-oxide ligands mbpymNO (**2**) and phenNO (**3**) are significantly different in both cases because of the intrinsic nature of each ligand. In the mbpymNO ligand, the two pyrimidine moieties can rotate freely through the C5−C6 bond, whereas for the phenNO ligand, an equivalent rotation of the pyridine rings through the C11−C12 bond is not possible. Thus, in **2**, the pyrimidine rings of the mbpymNO ligand are twisted by 48.45° relative to each other (Figure S1a). In **1**, the simultaneous coordination of the ligand to two Dy^{III} centers forces the pyrimidine rings to adopt a conformation more planar than that in **2**. The Dy1−O1−N1 angle deviates strongly from linearity with a value of 122.0(3)°. For **3**, the phenNO ligand is slightly bent, with the dihedral angle between the planes containing the aromatic rings N2−C10−C9−C8−C7−C11 and C12−C4−C3−C2−C1−N1 only 11.17° (Figure S1b and Table S4). The N1−O1−Dy1 angle also deviates strongly from linearity [130.6(4)°] although to a lesser extent than in the cases of **1** and **2**.

The shortest intermolecular Dy−Dy distances are 9.084 Å for **2** and 9.309 Å for **3**, and although in both cases weak *π*−*π* interactions exist between the aromatic rings of the adjacent molecules, the Dy^{III} centers can be considered to be isolated from a magnetic point of view [shortest *π*−*π* distances are 3.649 Å for **2** and 3.609 Å for **3** (Figures S2 and S3 respectively)].

Magnetic Properties. Thermal variation of the dc magnetic data ($\chi_M T$ vs T plots) for complexes **1**−**3** (Figure S4) shows $\chi_M T$ values at T = 300 K of 27.59 cm^3 K mol^{-1} (**1**), 13.68 cm^3 K mol^{-1} (**2**), and 14.66 cm^3 K mol^{-1} (**3**), which are close to the theoretical value of 14.17 cm^3 K mol^{-1} per Dy^{III} ion in the free-ion approximation ($4f^9$, $J = {}^{15}/_2$, $S = {}^{5}/_2$, L = 5, $g = {}^{4}/_3$, $^6H_{15/2}$). Upon cooling, the $\chi_M T$ products decrease continuously to reach values of 21.04 cm^3 K mol^{-1} (**1**), 11.96 cm^3 K mol^{-1}(**2**), and 12.99 cm^3 K mol^{-1} (**3**) at 2 K. For the mononuclear complexes **2** and **3**, this behavior is due to the combined effects of thermal depopulation of the M_J sublevels of the $^6H_{15/2}$ ground term split by crystal-field effects and possible intermolecular dipolar interactions. For the dinuclear complex **1**, additional weak intramolecular antiferromagnetic exchange interactions between the Dy^{III} centers through the mbpymNO bridging ligand could be responsible for the sharp decrease in $\chi_M T$ at very low temperature. The M versus H plots at 2 K for complexes **1**−**3** show a rapid increase of the magnetization below 1 T and then a very slow linear increase to reach values of 9.88 Nμ_B (**1**) (4.94 Nμ_B per Dy^{III} ion), 5.89 Nμ_B (**2**), and 5.94 Nμ_B (**3**) at 5 T. These values are much lower than the expected saturation value of 10 Nμ_B per Dy^{III} ion (M_S/Nμ_B = $g_J J$ = 10 Nμ_B) and are compatible with the existence of strong

DOI: 10.1021/acs.inorgchem.8b00427
Inorg. Chem. 2018, 57, 6362−6375

crystal-field effects, leading to approximate axial symmetry with far-separated energy levels and, therefore, with a well-isolated $\pm^{15}/_{2}$ ground state.[6d]

SMM Behavior. As expected from the easy-axis anisotropy of the Dy^{III} ion (see below for ab initio calculations), complexes **1**−**3** show frequency and temperature dependence of the out-of-phase magnetic susceptibility (χ''_M) at zero field, which is indicative of slow relaxation of the magnetization and SMM behavior. For compound **1**, the temperature dependence of the χ'' plot shows a broad signal devoid of any neat maximum between 7 and 20 K, a clearly visible shoulder between 4 K (150 Hz) and 5 K (1400 Hz), and a relatively strong increase of χ''_M below 3 K (Figure S5). This behavior can be due to the overlap of different relaxation processes, including fast QTM relaxation, which is responsible of the strong increase of χ''_M at very low temperature. The QTM relaxation process dominates in intensity and, consequently, modulates the relative intensity of the other signals.

In order to eliminate entirely or partially the QTM, ac measurements were carried out in the presence of a small external dc field. To know the optimal magnetic field that induces a larger relaxation time, the frequency dependence of the ac out-of-phase signal at 3 K at different fields was analyzed to extract the relaxation times at each magnetic field. The field dependence of the relaxation times (Figure S6) clearly shows that τ increases until 1000 Oe and then remains almost constant. Therefore, ac measurements were carried out in the presence of an external dc field of 1000 Oe. Under these conditions, two maxima were observed in the 3.0 K (10 Hz)−5.5 K (1400 Hz) and 5.5 K (10 Hz)−13.5 K (1400 Hz) ranges, and the low-temperature tail due to QTM almost disappears (Figures 2a and S7). The presence of two relaxation processes SR (slow relaxation at high temperature) and FR (fast relaxation at low temperature) could be due to the existence of two different Dy^{III} centers in the structure. The fit of the Cole−Cole plot (Figure S8) to the Debye model with the *CCFIT* program[25] afforded the temperature dependence of the relaxation times for the SR and FR relaxation processes. The fit of these data to the Arrhenius law (Figure 2c) led to the following parameters U_{eff} = 54.7 K and $\tau_0 = 1.7(3) \times 10^{-6}$ s and U_{eff} = 47.8 K and $\tau_0 = 1.5(4) \times 10^{-8}$ s for the SR and FR relaxation processes, respectively.

At zero dc field, the mononuclear complexes **2** and **3** exhibit frequency and temperature dependence of the out-of-phase susceptibility signal (χ''_M) below 15 K (Figures S9a and S12a, respectively), which is indicative of slow relaxation of the magnetization and SMM behavior. However, the presence of an intense increase of the χ''_M signals below ∼7 K due to fast QTM precludes in both cases the observation of neat maxima.

When a 0.1 T external dc magnetic field was applied to cancel or reduce QTM (this is the optimal field for both compounds inducing a larger relaxation time; Figure S11), well-defined χ''_M signals appeared in both cases (Figures S9b and S12b, respectively). For **2**, the χ''_M maxima appear between 4.6 K (60 Hz) and 10.2 K (10000 Hz). For **3**, those maxima are slightly displaced to higher temperatures [6.25 K (10 Hz)−11.5 K (1400 Hz)]. Fitting of the frequency dependence of χ''_M at different temperatures to the generalized Debye model afforded the relaxation times of the magnetization (τ) at each temperature (Figure 3). The effective energy barrier for the reversal of the magnetization (U_{eff}) and the preexponential factor τ_0 calculated from the fit of τ to an Arrhenius law were

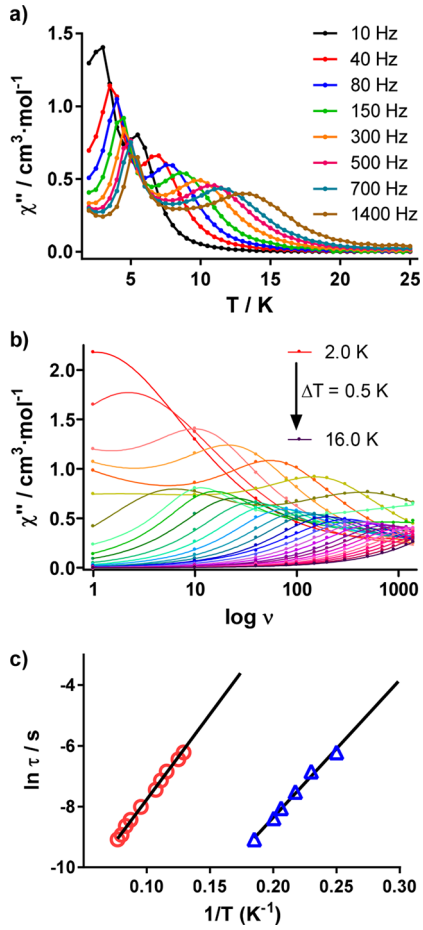

Figure 2. Temperature (a) and frequency (b) dependence of out-of-phase ac susceptibility signals at 1000 Oe for complex **1**. Solid lines are only guide for the eyes. Arrhenius plots (c) for slow (red circles) and fast (blue triangles) relaxation processes for complex **1**.

U_{eff} = 71.5 (5) K and $\tau_0 = 1.9(2) \times 10^{-8}$ s and U_{eff} = 120.7(4) K and $\tau_0 = 3.9(4) \times 10^{-9}$ s for **2** and **3**, respectively.

The deviation of the data from the Arrhenius law at low temperatures is indicative of the existence of several competing relaxation processes. The Cole−Cole plots for these complexes show semicircular shapes [Figures S10 (**2**) and S13 (**3**)], with α values ranging between 0.164 (5.6 K) and 0.202 (10.6 K) for **2** and 0.215 (7 K) and 0.218 (12 K) for **3**, which support the existence of several relaxation processes in both cases. Because in the temperature ranges studied (T > 6 K and 0.1 T) QTM and direct relaxation processes are expected to be almost negligible, we fitted the magnetic data to eq 1, which considers that Raman and Orbach processes contribute simultaneously to the relaxation of the magnetization.

$$\tau^{-1} = BT^{n} + \tau_0^{-1} \exp(-U_{eff}/k_B T) \quad (1)$$

The extracted parameters were B = 0.24, n = 4.9, U_{eff} = 99.6 K, and $\tau_0 = 2.1 \times 10^{-9}$ s for **2** and B = 0.005, n = 5.2, U_{eff} = 159.1 K, and $\tau_0 = 1.9 \times 10^{-10}$ s for **3**. The U_{eff} values are higher than those obtained from the simple Arrhenius law, while the preexponential factors τ_0 decrease by almost 1 order of magnitude.

Ab Initio Calculations. In order to confirm the axial anisotropy of the ground state and to gain insight into the mechanism of the slow magnetic relaxation of **1**−**3**, we performed electronic calculations on their X-ray structures

DOI: 10.1021/acs.inorgchem.8b00427
Inorg. Chem. 2018, 57, 6362−6375

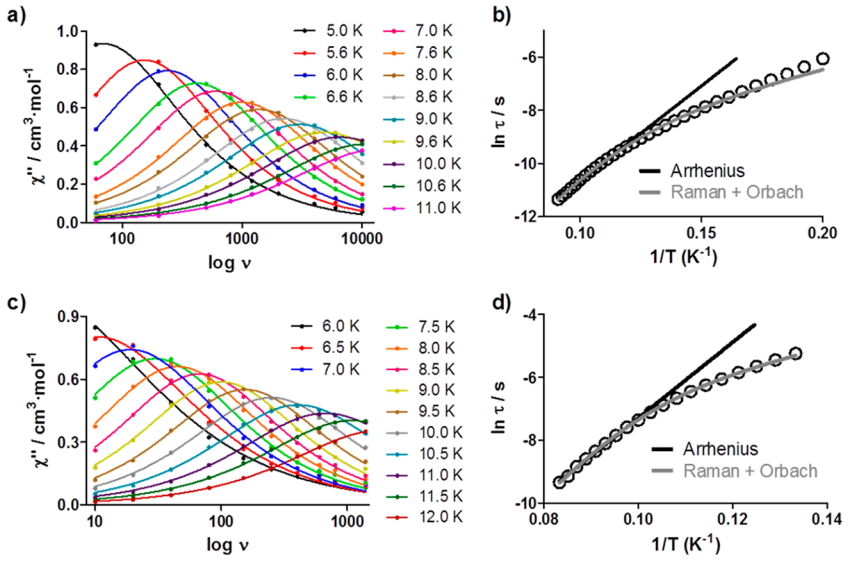

Figure 3. Frequency dependence of the out-of-phase susceptibility signal χ''_M of complexes **2** (a) and **3** (c) at different temperatures under an optimized applied dc field of 0.1 T. The solid lines represent the best fits to the Debye model. ln τ versus T^{-1} plot for complexes **2** (b) and **3** (d). The solid lines represent the best fits of the experimental data to the Arrhenius law for a thermally activated process (black line) or to an Orbach/Raman relaxation process (gray line).

based on the CASSCF+RASSI-SO/*SINGLE_ANISO* method[19] using the *MOLCAS 8.0* code.[16] The energy spectrum, **g** tensors, and wave functions for the eight Kramers doublets (KDs) arising from the splitting of the ground-state $^6H_{15/2}$ spin−orbit atomic term, which is induced by the CF in compounds **1**−**3**, are gathered in Tables 1, 2, and S6−S9.

Table 1. CASSCF+RASSI-Calculated Energies for the Eight KDs Stemming from the Ground-State $^6H_{15/2}$ Multiplet for Compounds 1−3 (Method I)

	energy (cm^{-1})			
KD	**1-Dy1**	**1-Dy2**	**2**	**3**
1	0.0	0.0	0.0	0.0
2	109.78	157.20	82.26	140.69
3	144.24	232.53	130.72	200.43
4	202.47	273.49	153.89	230.11
5	256.20	316.34	188.04	261.71
6	281.69	395.47	260.96	337.82
7	443.79	468.42	291.77	368.75
8	571.47	553.03	423.15	483.71

Table 2. *g* Factors and Wave Function for the Ground-State KD of Compounds 1−3 (Method I)

compound	g_x	g_y	g_z	wave function
1-Dy1	0.04	0.07	19.68	$0.98\|\pm^{15}/_2\rangle + 0.02\|\pm^{13}/_2\rangle$
1-Dy2	0.01	0.01	19.52	$0.94\|\pm^{15}/_2\rangle + 0.04\|\pm^{11}/_2\rangle$
2	0.02	0.03	18.92	$0.93\|\pm^{15}/_2\rangle + 0.07\|\pm^{3}/_2\rangle$
3	0.00	0.00	19.58	$0.96\|\pm^{15}/_2\rangle + 0.03\|\pm^{11}/_2\rangle$

For compound **1**, the calculated energy spectra of the eight KDs span up to 571 and 553 cm^{-1}, with subsequent excited-state spin−orbit terms lying at 3050 and 3066 cm^{-1} for the Dy1 and Dy2 sites, respectively. The anisotropy of the ground-state Kramers doublet state (KD1) for both Dy sites (Dy1 and Dy2) is of the pure Ising type, as indicated by the large magnetic moments with g_z approaching the ideally pure $m_J = \pm^{15}/_2$ state (g_z = 20; Tables 2 and S6 and S7), which favors slow relaxation of the magnetization and SMM behavior.[26] The Ising nature of the ground state is also supported by the corresponding wave functions. Thus, the wave functions associated with KD1 are almost pure $|\pm^{15}/_2\rangle$ for both Dy sites, whereas those associated with KD2 show a high degree of mixing (Tables 2 and S6 and S7). Comparatively, the associated transverse component is larger for the Dy2 site compared to the Dy1 site for all of the KDs including the ground state. This clearly implies a nonsymmetric nature of the two Dy sites within complex **1**. It is worth noting that in both cases the axiality of the excited states decreases until the fourth KD with a proportional increase of the magnetic moment along the *XY* plane. From this KD, the axiality increases again gradually to reach an almost pure Ising type in the eighth KD, thus replicating the anisotropy of the ground state (KD1; Tables S6 and S7). This mirror symmetry explicitly represents systems possessing low symmetry around the metal ions. KD1 is found to possess a zero magnetic moment in the *XY* plane, and it is entirely oriented along the *Z* axis.

The calculated magnetic moment of the ground state for Dy1 and Dy2 (Figure 4) lies close to the two tmh β-diketonato ligands on the opposite sides of each Dy atom, which provide an appropriate axial crystal field, with the remaining positions in the equatorial plane occupied by the O atoms of the other tmh bidentate ligand and the N,N or N,O atoms belonging to the neutral bis-bidentate mbpymNO ligand. In this disposition, the oblate electron density of the Dy^{III} ion is forced to be located in the equatorial plane, thus diminishing the electrostatic repulsions with the O atoms of the two β-diketonato ligands defining the axial crystal field and the anisotropic axis, as was qualitatively predicted with the oblate−prolate model.[27] In fact, the deviation of the ab initio computed ground-state g_{zz} orientation with respect to the electrostatic anisotropy axis (Figure S14) is actually very small.

It is worth remembering that magnetic relaxation in lanthanides is found to take place fundamentally through the following pathways in the absence of intermolecular interactions:[28,29] (i) QTM within the ground-state KD1, which arises from its large transverse anisotropy, (ii) Orbach/Raman

DOI: 10.1021/acs.inorgchem.8b00427
Inorg. Chem. 2018, 57, 6362−6375

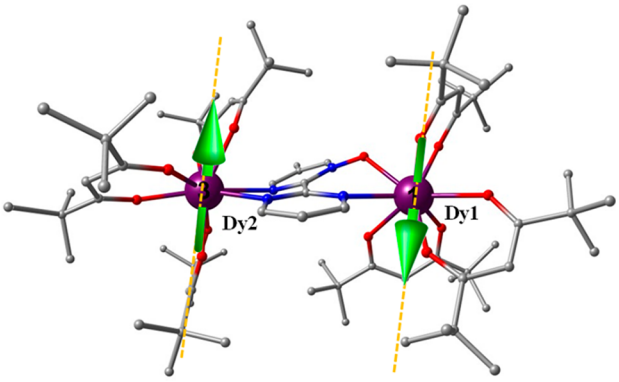

Figure 4. Crystal structure of complex **1** showing the ab initio computed principal anisotropy direction (g_{zz}) of both Dy sites in their ground-state KDs, as procured from approach I.

processes, which account for the relaxation via excited-state KDs promoted fundamentally by the noncoincidence of the principal anisotropic axes, (iii) thermally assisted QTM (TA-QTM) via excited-state KDs due to their non-Ising nature. The magnitudes of these spin-phonon relaxations depend on the square of the transverse magnetic moment. In view of this and with the aim of revealing the magnetic relaxation pathways of Dy1 and Dy2 in compound **1**, we have calculated the mean absolute values of the transverse magnetic moments between the connecting pairs of opposite magnetization. The qualitative mechanism of relaxation obtained from ab initio calculations for **1** and for both Dy^{III} sites is shown in Figure 5. Here the states are arranged according to the values of their magnetic moments. The number at each arrow connecting any two states is the mean absolute value of the matrix elements of the transition magnetic moments between the corresponding states. The pure Ising nature of the ground-state anisotropy (g_{zz} values of 19.68 and 19.52 respectively for the Dy1 and Dy2 sites) induces almost completely suppressed QTM in both Dy^{III} ions in **1** [the matrix element of the transition magnetic moment is 0.02 μ_B (Dy1) and 0.003 μ_B (Dy2), and an efficient spin relaxation mechanism is only expected when the transition magnetic moment is above 0.1 μ_B].[30]

For both centers, the first excited-state KD (KD2) shows considerable transverse anisotropy, leading to relaxation via this state. The energy gap between the first excited- and ground-state KD (KD2 − KD1) is computed to be 109.8 and 157.2 cm^{-1} for the Dy1 and Dy2 sites, respectively. This outlines the existence of two different relaxation phenomena, corroborating the experimental ac magnetic measurements. Moreover, substantial misalignment of the first excited-state g_{zz} axis with respect to that in the ground state, particularly for the Dy1 site (67° for Dy1 and 17.2° for Dy2) reinforces the magnetic relaxation via the first excited state. This is strongly supported by our computed spin-phonon relaxation (Orbach/Raman) contribution from KD2 as 1.16/0.38 and 1.89/0.03 for the Dy1 and Dy2 sites, respectively. Relaxation occurrence within this KD2 state is further corroborated by the significant tunnelling contribution (TA-QTM as 0.77 μ_B and 0.17 μ_B for Dy1 and Dy2, respectively). In view of the above considerations and taking into account that the blocking barrier is determined by the closest pathways with larger transition magnetic moments,[31] both Orbach and TA-QTM relaxations via the first excited-state KD2 are operative. However, higher axiality, lower transverse anisotropy, and smaller matrix elements corresponding to QTM and TA-QTM contribute to comparatively greater barrier values for the individual Dy2 center compared to Dy1. However, the calculated energy gaps for Dy1 and Dy2 that determine the thermal energy barriers are rather higher that those extracted from the experimental results, assuming a value of 33 cm^{-1} for Dy1 and 38 cm^{-1} for Dy2, corresponding to the FR and SR relaxation processes, respectively (irrespective of the used method, either I or II, calculations indicated a smaller U_{eff} for the Dy1 center; therefore, it is reasonable to assume the low experimental U_{eff} for this Dy1 center). This deviation between the calculated and experimental results is rather usual and could be due, among other factors, to (i) the existence of additional relaxation pathways, particularly QTM in the ground state promoted by dipolar and hyperfine interactions, which reduces the expected pure Orbach thermal energy barrier to an effective value (U_{eff}), (ii) limitations inherent to the computational tool, and (iii) possible modifications occurring in the structure at very low temperature.

Although calculations indicate negligible QTM, the experimental results (Figure S5) show that at zero-field QTM is the dominant relaxation process at low temperature, probably because of intermolecular and/or hyperfine interactions, which are known to favor this type of relaxation. In order to suppress the intermolecular dipolar interactions, we prepared a magnetically diluted analogue of **1** using a Dy/Y = 1/10 molar ratio (**1′**). The ac measurements on **1′** at zero dc field and 1200 Hz show that the QTM is only partly suppressed because a net maximum and a shoulder are clearly visible at almost the same temperatures as those for **1** measured in the presence of a dc field of 1 kOe. Moreover, an intense tail due to QTM is observed below 5 K. When ac measurements on **1′** are

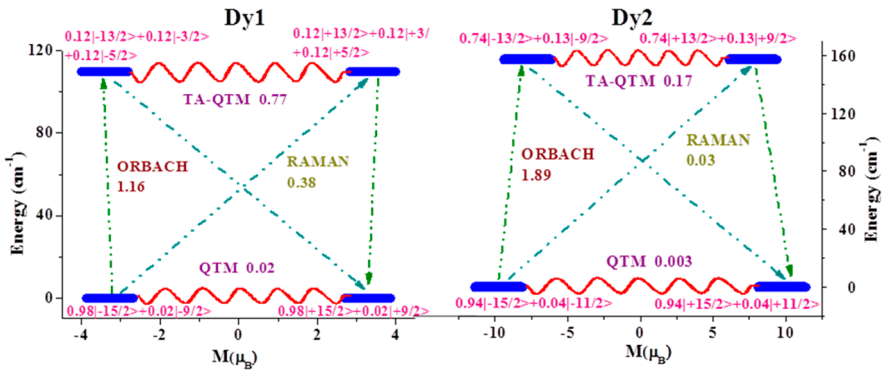

Figure 5. Ab initio computed relaxation mechanism for both Dy^{III} sites in complex **1** (method I).

DOI: 10.1021/acs.inorgchem.8b00427
Inorg. Chem. 2018, 57, 6362−6375

performed in the presence of a magnetic field of 1 kOe (Figure S15), both χ''_M peaks for the SR and FR processes do not appreciably shift with respect to their positions in the neat compound **1** at 1 kOe. However, the very small tail at very low temperature for **1** at 1 kOe due to QTM disappears, as expected from the reduction of the intermolecular dipolar interactions after magnetic dilution. In view of the above evidence, it seems to be clear that the magnetic field is more effective than dilution in quenching the QTM in **1**.

To better understand the relaxation mechanism, we attempted to use computed crystal-field parameters. The corresponding crystal-field Hamiltonian is given as $H_{CF} = B_k^q O_k^q$, where B_k^q is the crystal-field parameter, while O_k^q is Steven's operator (Table S10). The axial parameter B_k^q (where $k = 0$ and $q = 2$) is comparatively larger for the Dy2 ion (−1.93) compared to the Dy1 site (−1.66). This strongly correlates to our computed barrier height and underlines the influence of the ligand-field strength in U_{eff}.

Until now, we have only discussed the single-ion analysis/behavior of two individual Dy centers in complex **1**; now we intend to understand its exchange-coupled behavior. The computed g_{zz} values of the individual Dy^{III} fragments are close to 20. This implies that Dy^{III}−Dy^{III} exchange coupling can be regarded as Ising type. The *POLY_ANISO* program was harnessed to fit magnetic susceptibility and magnetization data considering the exchange parameters within the Lines approach. The magnetic interactions can be depicted by $H = -Js_{1z1}s_{2z2}$, where s_{1z1} and s_{2z2} represent projections of the effective spin $\tilde{s} = {}^1/_2$ of the lowest KDs of the Dy^{III} ions on the principal anisotropy axes. The fitting then yielded J_{tot} as −0.07 cm^{-1} (J_{exch} = −0.04 cm^{-1} and $J_{dip.}$ = −0.03 cm^{-1}).

The main magnetic axis and local magnetization vectors on the Dy^{III} centers lie antiparallel to each other, and this is in compliance with antiferromagnetic Dy^{III}−Dy^{III} coupling within the Lines model (Figure 4). Considerable tunnelling transition between the third exchange doublets (∼10^{-5} cm^{-1}) enacted efficiently to block the magnetization through that level (Figure 6; see also the Supporting Information for a detailed discussion) lying at ∼109 cm^{-1} above the ground state. Weaker exchange coupling between the two Dy centers undermines the impact of the coupled system on the magnetic anisotropy. This is witnessed by the observed magnetization blockade in a {Dy2} coupled complex (∼109 cm^{-1}), which resembles the barrier obtained from single-ion analysis. Therefore, the first two close-lying exchange spectra (expanded within 0.48 cm^{-1}; Figure 6) and weaker Dy−Dy interaction (<1 cm^{-1}) postulate that an experimentally observed barrier likely arises from individual Dy^{III} fragments/centers.[32]

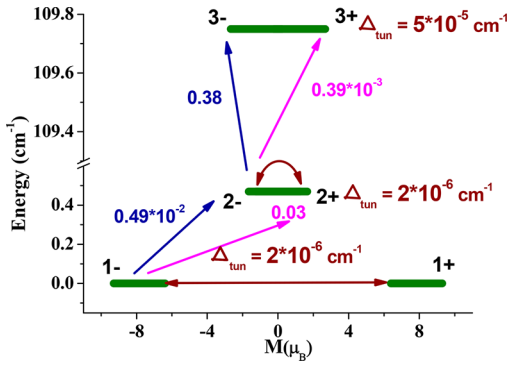

Figure 6. Low-lying exchange spectrum (relative to the energy of the ground state) and the position of the magnetization blockade barrier (red dashed line) in the Dy_2 complex **1** employing approach I. The bold green lines indicate exchange states that have been arranged in compliance with the value of its magnetic moment. The brown-red arrows (and pertinent values) correspond to tunnelling transitions within ground-state and first excited-state exchange doublets. However, blue and pink arrows and their corresponding values represent transition magnetic moment matrix elements of spin-phonon relaxation pathways.

For complexes **2** and **3**, the energy separation values between KD1 and KD8 are 423 and 483 cm^{-1}, respectively, whereas the next excited-state spin−orbit term is located at 3600 cm^{-1} for **2** and at 3053 cm^{-1} for **3** (Tables S8 and S9). In both complexes, the Dy^{III} centers also exhibit a ground state with anisotropy of the pure Ising type and large magnetic moments with **g**-tensor values close to those of an ideally pure $M_J = \pm{}^{15}/_2$ state (g_z = 20; $g_x = g_y = 0$). Nevertheless, the axiality of the ground state (KD1) is higher for **3**, and as a consequence, its wave function is closer to pure $|\pm{}^{15}/_2\rangle$. For these complexes, the axiality decreases from KD1 to KD4 and increases from the latter to KD8, leading to Ising-type anisotropy again at KD8. In both cases, the calculated magnetic moment of the ground state (Figures 7 and 8) lies close to the two β-diketonato ligands at the opposite sides of each Dy atom, as expected. The qualitative mechanisms of relaxation obtained from ab initio calculations for **2** and **3** are shown in Figures 7 and 8, respectively, together with the computed transverse magnetic moments between the connecting pairs of opposite magnetization.

For complexes **2** and **3**, QTM in the ground state is not active because the zero transverse magnetic moments are almost negligible (∼10^{-2} μ_B, which significantly reduces the probability of QTM relaxation). In spite of this, the experimental results (Figures S9 and S12) show that, at zero field, QTM is the prevailing relaxation process at low temperature. Even in the presence of a dc field of 1 kOe, a small tail below 3 K is observed for complex **2**. To suppress intermolecular dipolar interactions, which favor QTM, Dy/Y = 1/20 diluted versions of **2** and **3** were prepared (**2′** and **3′**). The ac measurements on **2′**and **3′** at zero dc field and 1200 Hz (Figures S17 and S18) clearly show that the tiny tail observed at very low temperature for **2** at 1 kOe, due to QTM, vanishes as a result of the drop of the intermolecular dipolar interactions following magnetic dilution. Moreover, the peaks observed in the temperature dependence of the χ''_M signals for both diluted complexes do not appreciably shift with respect to their positions in the neat compounds at 1 kOe. In this case, the effect of the dilution on the QTM relaxation is similar to that induced by the magnetic field.

The first excited-state g_{zz} axis for **2** and **3** is notably misaligned with regard to that in the ground state (11.57° and 7.86°, respectively), which underlines that the magnetic relaxation can be operative via the first excited state (KD2). This is strongly supported by the calculated spin-phonon relaxation (Orbach/Raman) contribution from the KD2 (2.14/0.05 and 1.86/0.01, respectively). The relaxation via KD2 is additionally corroborated by the significant tunnelling contribution (TA-QTM with transverse magnetic moments of 0.42 and 0.34 μ_B for **2** and **3**, respectively). The ground (KD1)−first excited state KD (KD2) gap is computed to be 83 cm^{-1} for **2** and 141 cm^{-1} for **3**. We have also computed crystal-field parameters for **2** and **3** (Table S12). A negative B_2^0 axial CF parameter corresponds to a favorable coordination environment, inducing ideal SMM behavior. The parameter B_2^0 for the

DOI: 10.1021/acs.inorgchem.8b00427
Inorg. Chem. 2018, 57, 6362−6375

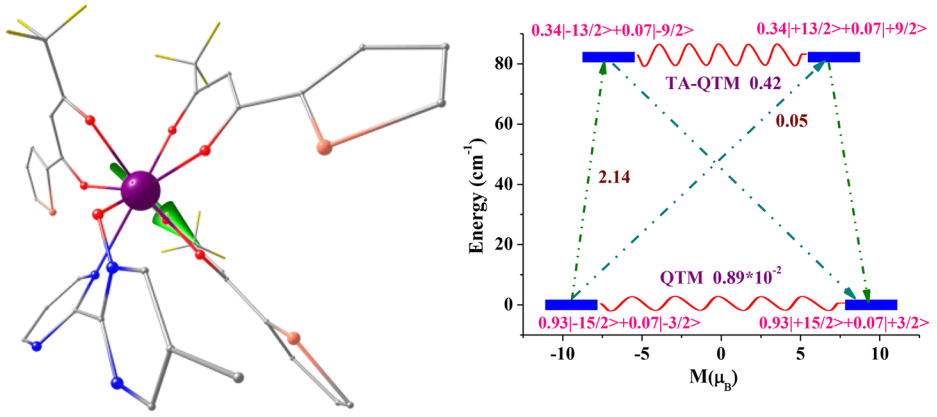

Figure 7. Crystal structure showing the principal anisotropy direction (g_{zz}) of the ground-state KD and ab initio computed relaxation mechanism for complex **2**.

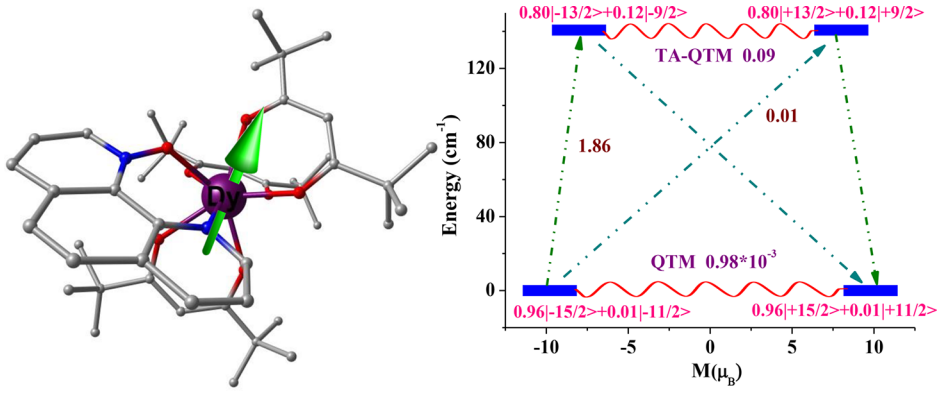

Figure 8. Crystal structure showing the principal anisotropy direction (g_{zz}) of the ground-state KD and ab initio computed relaxation mechanism for complex **3**.

Dy site in **2** (−0.14) is significantly lower than that of the Dy site in **3** (−0.77). This agrees well with the fact that the computed energy barrier for **3** is significantly higher than that shown by **2**.

A comparison of the experimental U_{eff} of complexes **1**−**3** (33 and 38 cm^{-1} for Dy1 and Dy2 in complex **1** and 49.6 and 83.4 cm^{-1} for **2** and **3**) with those calculated theoretically reveals that U_{eff} for the latter are, as usual, higher than the former ones. Although the theoretical U_{eff} values for sites Dy1 and Dy2 in complex **1** follow the same trend as the experimental ones, the absolute values are overestimated (109.8 and 157.2 cm^{-1}, respectively). To see if this overestimation could be due to the methodology employed, we have performed calculations with approach II (see the computational details), and here KD1 is found to be slightly less axial (Tables S13 and S14) with the energy gap between KD1 and KD2 (U_{cal}) estimated to be 76.29 cm^{-1} (for the Dy1 site) and 96.57 cm^{-1} (for the Dy2 site) (see Tables S13 and S14 and Figure S20). The values estimated by this approach are slightly lower than the earlier ones and move toward the experimental estimate, but still in absolute magnitude, the values are overestimated (Figures S19 and S20 and Tables S13−S15).

In general, to generate a high-energy barrier, leading to slow magnetic relaxation and SMM behavior, a ground state with higher M_J is desired. In the case of the Dy^{III} ion, this condition can be attained with an axial coordination environment that enhances the electron density close to the axis. For eight-coordinated complexes with almost equivalent donor atoms and similar Dy−ligand distances, an axially elongated square-antiprism coordination sphere (D_{4d}) favors the existence of a large energy barrier for magnetization reversal with an almost pure M_J wave function in the ground state. Deviations from this symmetry provoke the mixing of M_J wave functions in the ground doublet state, which favors the fast quantum tunnelling of the magnetization that reduces or fully eliminates the energy barrier. Low-symmetry Dy^{III} complexes with different ligands and Dy−O distances generally exhibit easy-axis anisotropy in the ground-state KD, leading to a barrier for magnetization reversal and slow relaxation of the magnetization. In these cases, to reduce the repulsion with the closest coordinated atoms, the electron density of the $M_J = {}^{15}/_{2}$ state of Dy^{III} ground-state KD, the disk-shaped electron density is accommodated almost perpendicularly to the shortest Dy−O bond distances,[1b] so that the magnetic moment (which is perpendicular to the electron density disk) lies in the direction of the shortest Dy−O bonds. Nevertheless, in most cases, the ground-state wave functions are not pure M_J $|\pm{}^{15}/_{2}\rangle$ states but mixed with other lower M_J wave functions, leading to a fast QTM process at zero field that decreases the temperature at which magnetic hysteresis is observed. In view of these considerations, a good strategy to access SMM complexes in eight-coordinated Dy^{III} would be that of creating an axially elongated crystal field around the Dy^{III} center (preferably of square-prismatic geometry) by placing the ligands with the shorter Dy−O distances at the opposite sides of each Dy atom and the remaining atoms at the equatorial plane. Complexes **1**−

DOI: 10.1021/acs.inorgchem.8b00427
Inorg. Chem. 2018, 57, 6362−6375

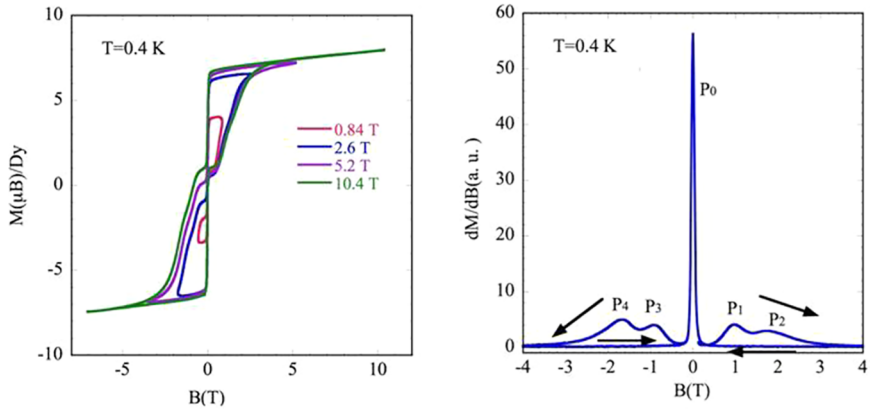

Figure 9. Pulsed-field magnetization curves at maximum fields of 0.84, 2.6, 5.2, and 10.4 T (left) and a differential of magnetization measured at 0.4 K (right) for compound **1**.

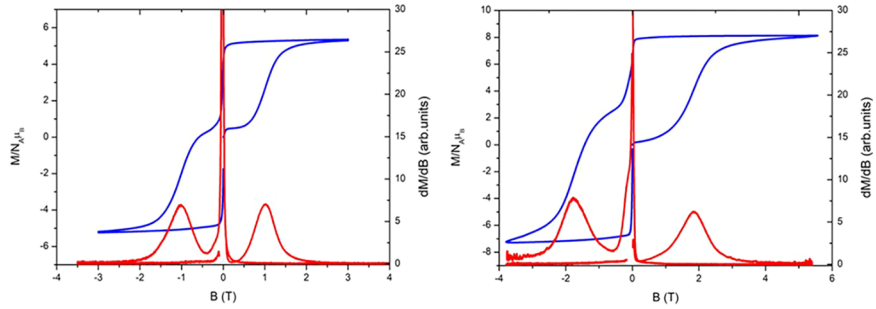

Figure 10. Pulsed-field magnetization curves at a maximum field of 10.4 T and a differential of magnetization measured at 0.4 K for compounds **2** (left) and **3** (right).

3 obey this criterium because they have two β-diketonato ligands at the opposite sides of each Dy atom, while the remaining positions in the equatorial plane are occupied by the O atoms of the other β-diketonato bidentate ligand and the N,N or N,O atoms belonging to the *N*-oxide ligands. This configuration generates, as indicated elsewhere, an appropriate axial crystal field because the Dy−O bond distances belonging to the β-diketonato ligand are the shortest ones and similar to the Dy−O distance of the *N*-oxide group. The two β-diketonato ligands at the opposite sides of each Dy^{III} atom create a "pseudo axis", with the magnetic moment lying close to it. Theoretical and experimental studies have revealed that distortion of the local coordination environment of the Dy^{III} ion from ideal geometry can significantly affect the magnetization relaxation dynamics.[26b,33,34] In fact, for eight-coordinated Dy^{III} SMM complexes, distortion from square-antiprismatic to triangular-dodecahedral geometry promotes a reduction of the energy barrier.[35] The calculated energy barriers (energy gap between the KD1 and KD2 doublets) for the Dy^{III} ions linked to the N,O bidentate part of the ligands in complexes **1**−**3** follow this trend because *U* values decrease with distortion from the square-antiprism geometry quantified by the shape-measures parameter (*S*): 0.55 (141 cm^{-1}) for **3**, 0.79 (82.3 cm^{-1}) for **2**, and 1.70 (76 cm^{-1}, approach II) for **1**. Although rather smaller than the calculated values, the experimental ones follow the same order: 83.8 cm^{-1} for **3**, 49.6 cm^{-1} for **2**, and 33 cm^{-1} for **1**. In conclusion, the ground-state KDs in **1** (method II) seem to possess greater transverse anisotropy (Tables S13 and S14) than those of **2** and **3** (method I ; Tables S8 and S9). Additionally, transversal matrix elements pertaining to QTM are larger for Dy1 in **1** (Figure S20), rendering diminution of the U_{eff} values for **2** and **3** (Figures S7 and S8).

Pulse Magnetization Measurements. In order to confirm the SMM properties of **1**−**3**, we have measured the magnetization curve in a full cycle pulsed magnetic field at 0.4 K,[36] with maximum fields of 0.84, 2.6, 5.2, and 10.4 T. It should be noted that the average sweep rate depends on the maximum field and therefore is higher for 10.4 T (average sweep rate = 4.2 T ms^{-1}). Magnetization curves (Figure 9 for compound **1** and Figure 10 for compounds **2** and **3**) show large hysteresis loops, a sharp reversal around zero field, and saturation at high fields. The hysteresis increases with increasing sweeping rate, which is typical of SMMs. The reduction for the saturation moment per Dy ion from the expected value (10 $\mu\beta$/f.u.) can be mainly caused by the tilt between the local magnetization directions of the Dy1 and Dy2 ions and imperfect alignment in the field. Also, the sharp reversal around zero indicates that there is an adiabatic magnetization reversal presumably caused by the fast tunnelling process with a small tunnelling gap. The possible cause of the gap is inferred to be hyperfine interactions and/or transverse components of the magnetization by the low symmetry around the Dy^{III} ion. The contribution of weak intermolecular interactions should less significant because the sharp reversals are observed to be in common for the three complexes. This means that the pulse magnetization behavior for **1**−**3** is a single-molecule property.

To examine the origin of the loop, the differential magnetization d*M*/d*B* is plotted (Figures 9, right, 10, and S21).

For **1**, in the initial up-sweep, the magnetization first increases slowly and then shows two peaks, P1 and P2. These two peaks correspond to two steps in the magnetization

DOI: 10.1021/acs.inorgchem.8b00427
Inorg. Chem. 2018, 57, 6362−6375

curve. In the down-sweep from the magnetic field peak to the zero field, dM/dB is very small and the magnetization curve is nearly flat. The characteristic loop structure on the positive-field side shows that there are two barriers with different magnitudes, and thus the release field of the trapped magnetization splits in two. The existence of two barriers is also found as a double peak structure in χ''. After the sharp drop of the magnetization at around zero field, the magnetization stays around zero. Then the magnetization curve in the negative-field side is symmetric to that in the positive-field side. In the initial sweep from the zero field to the negative maximum, we found two peaks, P3 and P4, in dM/dB.

The sweep rate dependence of peaks P1−P4 (Figure S22) indicates that the magnetization behavior is symmetric for the magnetic field reversal, as is found in the magnetization curve. There is slight sweep rate dependence of the peak field. It is presumably caused by the balance between the thermal relaxation time and the short sweeping time. The occurrence of a two-step magnetization curve in the dinuclear complex **1** and the presence of only one step for the mononuclear complexes **2** and **3** (Figure 9) point out that the two barriers in complex **1** can be caused by the sizable magnetic coupling between two Dy ions. Nevertheless, these two barriers could also appear to be due to the nonequivalence of Dy1 and Dy2 when magnetic coupling through the bridging ligand is negligible.

It should be remarked that hysteresis is larger for **3** than for **2**, which matches well with the fact that the theoretical and experimental U_{eff} values for the former are significantly larger than those for the latter.

CONCLUSIONS

The dissymmetric bridging ligand mbpymNO allows the design of the nonsymmetric dinuclear Dy^{III} complex **1**, exhibiting two different Dy1 and Dy2 sites, which are related to the N^O and N^N chelating sites of the ligand, respectively. ac magnetic measurements reveal the existence of two different slow magnetic relaxation processes associated with Dy1 and Dy2 with effective thermal energy barrier values of 47.8 K (FR) and 54.7 K (SR), respectively. The fact that Dy1 shows a higher distortion from an ideal D_{4d} geometry than Dy2 could justify why U_{eff} (Dy1) < U_{eff} (Dy2). Ab initio studies indicate that the ground state of both sites is of the Ising type and support the existence of two relaxation processes with computed energy gaps between the ground- and first excited-state KDs of 76 cm^{-1} (Dy1) and 97 cm^{-1} (Dy2). Additionally, two mononuclear SMM complexes were prepared from the mbpymNO (**2**) and phenNO (**3**) ligands. In both cases, the Dy(β-diketonate)$_3$ moieties are chelated to the N^O coordination site of the ligands and SMM is observed with U_{eff} values of 49.6 cm^{-1} for **2** and 83.4 cm^{-1} for **3**. Analysis of the structural and SMM properties of the Dy^{III} units linked to the N^O site of the ligands in **1**−**3** demonstrates that U_{eff} increases as the symmetry of the Dy(NO_7) coordination sphere approaches ideal D_{4d} symmetry. Pulse magnetization measurements support the SMM behavior of **1**−**3**. As expected, differential magnetization dM/dB curves for the dinuclear Dy^{III} complex **1** exhibit hysteresis loops with a double-step structure, whereas those for the mononuclear complexes **2** and **3** only display one step.

ASSOCIATED CONTENT

Supporting Information

The Supporting Information is available free of charge on the ACS Publications website at DOI: 10.1021/acs.inorgchem.8b00427.

Crystallographic data, selected bond distances and angles and tabulated continuous shape measures for complexes **1**−**3**, calculated energy spectra, **g** tensors, and angles between the anisotropy axes of the first excited and ground states, *SINGLE_ANISO*-computed crystal-field parameters, crystallographic structures emphasizing the dihedral planes between the aromatic rings in complexes **1**−**3** and the existence of $\pi-\pi$ interactions between the aromatic rings in complexes **2** and **3**, experimental and calculated $\chi_M T$ versus T and M versus H plots, plots showing the frequency dependence of χ_M and χ''_M at H_{dc} = 0 Oe, field dependence of the relaxation times at different H_{dc} fields and Cole−Cole plots for complexes **1**−**3**, thermal dependence of χ''_M at H_{dc} = 0.1 T for magnetically diluted complexes **1′** and **2′**, electrostatically calculated magnetic anisotropy axes for the Dy1 and Dy2 centers in **1**, differential of magnetization curves at different fields measured at T = 0.4 K for complex **1**, and theoretical analysis of magnetic relaxation in the Dy2 dinuclear system **1** (PDF)

AUTHOR INFORMATION

Corresponding Authors

*E-mail: jmherrera@ugr.res.
*E-mail: India.rajaraman@chem.iitb.ac.in.
*E-mail: nojiri@imr.tohoku.ac.jp.
*E-mail: ecolacio@ugr.es.

ORCID

Juan Manuel Herrera: 0000-0002-9255-227X
Daniel Aravena: 0000-0003-3140-4852
Eliseo Ruiz: 0000-0001-9097-8499
Gopalan Rajaraman: 0000-0001-6133-3026

Notes

The authors declare no competing financial interest.

ACKNOWLEDGMENTS

I.F.D.-O., J.M.H., E.R., and E.C. are grateful to the Ministerio de Economía y Competitividad and EU Feder Funds (Projects CTQ2014-56312-P and CTQ2015-64579-C3-1-P), the Junta de Andalucía (Grant FQM-195 and the Project of Excellence P11-FQM-7756), and the University of Granada for financial support. Part of this work was performed at the HFLSM, IMR, Tohoku University. I.F.D.-O. also acknowledges support by COLABS. G.R. and T.G. thank DST-SERB (Grant EMR/2014/00024) for funding. E.R. thanks the Generalitat de Catalunya for an ICREA Academia award.

REFERENCES

(1) Some reviews: (a) Gatteschi, D.; Sessoli, R.; Villain, J.; *Molecular Nanomagnets*; Oxford University Press: Oxford, U.K., 2006. (b) Rinehart, J. D.; Long, J. R. Exploiting single-ion anisotropy in the design of f-element single-molecule magnets. *Chem. Sci.* **2011**, *2*, 2078−2085. (c) Guo, Y. N.; Xu, G. F.; Guo, Y.; Tang, J. Relaxation dynamics of dysprosium(iii) single molecule magnets. *Dalton Trans.* **2011**, *40*, 9953−9963. (d) Sorace, L.; Benelli, C.; Gatteschi, D. Lanthanides in molecular magnetism: old tools in a new field. *Chem. Soc. Rev.* **2011**, *40*, 3092−3104. (e) Luzon, J.; Sessoli, R. Lanthanides

DOI: 10.1021/acs.inorgchem.8b00427
Inorg. Chem. 2018, 57, 6362−6375

in molecular magnetism: so fascinating, so challenging. *Dalton Trans.* **2012**, *41*, 13556−13567. (f) Clemente-Juan, J. M.; Coronado, E.; Gaita-Ariño, A. Magnetic polyoxometalates: from molecular magnetism to molecular spintronics and quantum computing. *Chem. Soc. Rev.* **2012**, *41*, 7464−7478. (g) Woodruff, D. N.; Winpenny, R. E. P.; Layfield, R. A. Lanthanide Single-Molecule Magnets. *Chem. Rev.* **2013**, *113*, 5110−5148. (h) Zhang, P.; Guo, Y.-N.; Tang, J. Recent advances in dysprosium-based single molecule magnets: Structural overview and synthetic strategies. *Coord. Chem. Rev.* **2013**, *257*, 1728−1763. (i) Layfield, R. A., Murugesu, M., Eds. *Lanthanides and Actinides in Molecular Magnetism*; Wiley-VCH: Weinheim, Germany, 2015. (j) Tang, J.; Zhang, P. *Lanthanide Single Molecule Magnets*; Springer-Verlag: Berlin, 2015; p 167. (k) Habib, F.; Murugesu, M. Lessons learned from dinuclear lanthanide nano-magnets. *Chem. Soc. Rev.* **2013**, *42*, 3278−3288. (l) Layfield, R. A. Organometallic Single-Molecule Magnets. *Organometallics* **2014**, *33*, 1084−1099. (m) Wang, B. W.; Gao, S. *The Rare Earth Elements, Fundamental and Applications*; Atwood, D. A., Ed.; John Wiley and Sons: New York, 2012. (n) Sessoli, R.; Powell, A. K. Strategies towards single molecule magnets based on lanthanide ions. *Coord. Chem. Rev.* **2009**, *253*, 2328−2341. (o) Andruh, M.; Costes, J. P.; Diaz, C.; Gao, S. 3d−4f Combined Chemistry: Synthetic Strategies and Magnetic Properties. *Inorg. Chem.* **2009**, *48*, 3342−3359. (p) Brechin, E. K. Introduction to the themed issue on molecular magnets. *Dalton Trans.* **2010**, *39*, 4671. (q) Sharples, J. W.; Collison, D. The coordination chemistry and magnetism of some 3d−4f and 4f amino-polyalcohol compounds. *Coord. Chem. Rev.* **2014**, *260*, 1−20. (r) Rosado Piquer, L.; Sañudo, E. C. Heterometallic 3d-4f single-molecule magnets. *Dalton Trans.* **2015**, *44*, 8771−8780. (s) Craig, G. A.; Murrie, M. 3d single-ion magnets. *Chem. Soc. Rev.* **2015**, *44*, 2135−2147. (t) Bartolomé, J.; Luis, F.; Fernández, J. F. *Molecular Magnets: Physics and Applications*; Springer-Verlag: Berlin, 2014. (u) Aromí, G.; Brechin, E. K. *Struct. Bonding (Berlin)* **2006**, *122*, 1. (v) Bagai, R.; Christou, G. The Drosophila of single-molecule magnetism: $[Mn_{12}O_{12}(O_2CR)_{16}(H_2O)_4]$. *Chem. Soc. Rev.* **2009**, *38*, 1011−1026. (w) Liddle, S. T.; van Slageren, J. Improving f-element single molecule magnets. *Chem. Soc. Rev.* **2015**, *44*, 6655−6669. (y) Frost, J. M.; Harriman, K. L. M.; Murugesu, M. The rise of 3-d single-ion magnets in molecular magnetism: towards materials from molecules. *Chem. Sci.* **2016**, *7*, 2470−2491. (z) Harriman, K. L. M.; Murugesu, M. An Organolanthanide Building Block Approach to Single-Molecule Magnets. *Acc. Chem. Res.* **2016**, *49*, 1158−1167.

(2) (a) Bogani, L.; Wernsdorfer, W. Molecular spintronics using single-molecule magnets. *Nat. Mater.* **2008**, *7*, 179−186. (b) Vincent, R.; Klyatskaya, S.; Ruben, M.; Wernsdorfer, W.; Balestro, F. Electronic read-out of a single nuclear spin using a molecular spin transistor. *Nature* **2012**, *488*, 357−360. (c) Ganzhorn, M.; Klyatskaya, S.; Ruben, M.; Wernsdorfer, W. Strong spin-phonon coupling between a single-molecule magnet and a carbon nanotube nanoelectromechanical system. *Nat. Nanotechnol.* **2013**, *8*, 165−169. (d) Jenkins, M.; Hümmer, T.; Martínez-Pérez, M. J.; García-Ripoll, J.; Zueco, D.; Luis, F. Coupling single-molecule magnets to quantum circuits. *New J. Phys.* **2013**, *15*, 095007. (e) Dediu, V. A.; Hueso, L. E.; Bergenti, I.; Taliani, C. Spin routes in organic semiconductors. *Nat. Mater.* **2009**, *8*, 707−716. (f) Prezioso, M.; Riminucci, A.; Graziosi, P.; Bergenti, I.; Rakshit, R.; Cecchini, R.; Vianelli, A.; Borgatti, F.; Haag, N.; Willis, M.; Drew, A. J.; Gillin, W. P.; Dediu, V. A. A Single-Device Universal Logic Gate Based on a Magnetically Enhanced Memristor. *Adv. Mater.* **2013**, *25*, 534−538. (g) Mannini, M.; Pineider, F.; Danieli, C.; Totti, F.; Sorace, L.; Sainctavit, P.; Arrio, M.-A.; Otero, E.; Joly, L.; Cezar, J. C.; Cornia, A.; Sessoli, R. Quantum tunnelling of the magnetization in a monolayer of oriented single-molecule magnets. *Nature* **2010**, *468*, 417−421. (h) Thiele, S.; Balestro, F.; Ballou, R.; Klyatskaya, S.; Ruben, M.; Wernsdorfer, W. Electrically driven nuclear spin resonance in single-molecule magnets. *Science* **2014**, *344*, 1135−1138. (i) Cornia, A.; Seneor, P. Spintronics: The molecular way. *Nat. Mater.* **2017**, *16*, 505−506. (j) Lumetti, S.; Candini, A.; Godfrin, C.; Balestro, F.; Wernsdorfer, W.; Klyatskaya, S.; Ruben, M.; Affronte, M. Single-molecule devices with graphene electrodes. *Dalton Trans.* **2016**, *45*, 16570−16574.

(3) (a) Rocha, A. R.; García-Suárez, V. M.; Bailey, S. W.; Lambert, C. J.; Ferrer, J.; Sanvito, S. Towards molecular spintronics. *Nat. Mater.* **2005**, *4*, 335−339. (b) Affronte, M. Molecular nanomagnets for information technologies. *J. Mater. Chem.* **2009**, *19*, 1731−1737.

(4) Sessoli, R.; Boulon, M.-E.; Caneschi, A.; Mannini, M.; Poggini, L.; Wilhelm, F.; Rogalev, A. Strong magneto-chiral dichroism in a paramagnetic molecular helix observed by hard X-rays. *Nat. Phys.* **2015**, *11*, 69−74.

(5) (a) Leuenberger, M. N.; Loss, D. Quantum computing in molecular magnets. *Nature* **2001**, *410*, 789−793. (b) Ardavan, A.; Rival, O.; Morton, J. J. L.; Blundell, S. J.; Tyryshkin, A. M.; Timco, G. A.; Winpenny, R. E. P. Will Spin-Relaxation Times in Molecular Magnets Permit Quantum Information Processing? *Phys. Rev. Lett.* **2007**, *98*, 057201. (c) Stamp, P. C. E.; Gaita-Ariño, A. Spin-based quantum computers made by chemistry: hows and whys. *J. Mater. Chem.* **2009**, *19*, 1718−1730. (d) Martínez-Pérez, M. J.; Cardona-Serra, S.; Schlegel, C.; Moro, F.; Alonso, P. J.; Prima-García, H.; Clemente-Juan, J. M.; Evangelisti, M.; Gaita-Ariño, A.; Sesé, J.; Van Slageren, J.; Coronado, E.; Luis, F. Gd-Based Single-Ion Magnets with Tunable Magnetic Anisotropy: Molecular Design of Spin Qubits. *Phys. Rev. Lett.* **2012**, *108*, 247213. (e) Ghirri, A.; Candini, A.; Affronte, M. Molecular Spins in the Context of Quantum Technologies. *Magnetochemistry* **2017**, *3* (1), 12.

(6) (a) Chen, Y.; Liu, J.; Ungur, L.; Liu, J.; Li, Q.; Wang, L.; Ni, Z.; Chibotaru, L. F.; Chen, X.; Tong, M. Symmetry-Supported Magnetic Blocking at 20 K in Pentagonal Bipyramidal Dy(III) Single-Ion Magnets. *J. Am. Chem. Soc.* **2016**, *138*, 2829−2837. (b) Gupta, S. K.; Rajeshkumar, T.; Rajaraman, G.; Murugavel, R. An air-stable Dy(III) single-ion magnet with high anisotropy barrier and blocking temperature. *Chem. Sci.* **2016**, *7*, 5181−5191. (c) Liu, J.; Chen, Y.; Jia, J.; Liu, J.; Vieru, V.; Ungur, L.; Chibotaru, L. F.; Lan, Y.; Wernsdorfer, W.; Gao, S.; Chen, X.; Tong, M. A Stable Pentagonal Bipyramidal Dy(III) Single-Ion Magnet with a Record Magnetization Reversal Barrier over 1000 K. *J. Am. Chem. Soc.* **2016**, *138*, 5441−5450. (d) Gregson, M.; Chilton, N. F.; Ariciu, A.-M.; Tuna, F.; Crowe, I. F.; Lewis, W.; Blake, A. J.; Collison, D.; McInnes, E. J. L.; Winpenny, R. E. P.; Liddle, S. T. A monometallic lanthanide bis(methanediide) single molecule magnet with a large energy barrier and complex spin relaxation behavior. *Chem. Sci.* **2016**, *7*, 155−165. (e) Ding, Y.-S.; Chilton, N. F.; Winpenny, R. E. P.; Zheng, Y.-Z. On Approaching the Limit of Molecular Magnetic Anisotropy:A Near-Perfect Pentagonal Bipyramidal Dysprosium(III) Single-Molecule Magnet. *Angew. Chem., Int. Ed.* **2016**, *55*, 16071−16074. (f) Chen, Y. C.; Liu, J. L.; Lan, Y.; Zhong, Z. Q.; Mansikkamäki, A.; Ungur, L.; Li, Q. W.; Jia, J. H.; Chibotaru, L. F.; Han, J. B.; Wernsdorfer, W.; Chen, X. M.; Tong, M. L. Dynamic Magnetic and Optical Insight into a High Performance Pentagonal Bipyramidal DyIII Single-Ion Magnet. *Chem. - Eur. J.* **2017**, *23*, 5708−5715. (g) Guo, F.-S.; Day, B. M.; Chen, Y.-C.; Tong, M.-L.; Mansikkamäki, A.; Layfield, R. A. A Dysprosium Metallocene Single-Molecule Magnet Functioning at the Axial Limit. *Angew. Chem., Int. Ed.* **2017**, *56*, 11445−11449. (h) Goodwin, C. A. P.; Ortu, F.; Reta, D.; Chilton, N. F.; Mills, D. P. Molecular magnetic hysteresis at 60 K in dysprosocenium. *Nature* **2017**, *548*, 439−442.

(7) (a) Ruiz, J.; Mota, A. J.; Rodríguez-Diéguez, A.; Titos, S.; Herrera, J. M.; Ruiz, E.; Cremades, E.; Costes, J. P.; Colacio, E. Field and dilution effects on the slow relaxation of a luminescent DyO_9 low-symmetry single-ion magnet. *Chem. Commun.* **2012**, *48*, 7916−7918. (b) Das, S.; Dey, A.; Biswas, S.; Colacio, E.; Chandrasekhar, V. Hydroxide-Free Cubane-Shaped Tetranuclear $[Ln_4]$ Complexes. *Inorg. Chem.* **2014**, *53*, 3417−3426. (c) Reis, S. G.; Briganti, M.; Soriano, S.; Guedes, G. P.; Calancea, S.; Tiseanu, C.; Novak, M. A.; del Águila-Sánchez, M. A.; Totti, F.; Lopez-Ortiz, F.; Andruh, M.; Vaz, M. G. F. Binuclear lanthanide-radical complexes featuring two centers with different magnetic and luminescence properties. *Inorg. Chem.* **2016**, *55*, 11676−11684.

(8) (a) Xue, S.; Ungur, L.; Guo, Y.-N.; Tang, J.; Chibotaru, L. F. Field-induced Multiple relaxation mechanism of $Co^{III}_2Dy^{III}_2$ compound with the Dysprossium ion in a Low-Symmetrical Environment. *Inorg. Chem.* **2014**, *53*, 12658−12663. (b) Habib, F.; Korobkov, I.;

DOI: 10.1021/acs.inorgchem.8b00427
Inorg. Chem. 2018, 57, 6362−6375

Murugesu, M. Exposing the intermolecular nature of the second relaxation pathway in a mononuclear cobalt(II) single-molecule magnet with positive anisotropy. *Dalton Trans.* **2015**, *44*, 6368−6373.
(9) (a) Yi, X.; Calvez, G.; Daiguebonne, C.; Guillou, O.; Bernot, K. Rational Organization of Lanthanide-Based SMM Dimers into Three-Dimensional Networks. *Inorg. Chem.* **2015**, *54*, 5213−5219. (b) Pointillart, F.; Le Guennic, B.; Golhen, S.; Cador, O.; Ouahab, L. Slow magnetic relaxation in radical cation tetrathiafulvalene-based lanthanide(III) dinuclear complexes. *Chem. Commun.* **2013**, *49*, 11632−11634. (c) Pointillart, F.; Le Guennic, B.; Cauchy, T.; Golhen, S.; Cador, O.; Maury, O.; Ouahab, L. A Series of Tetrathiafulvalene-Based Lanthanide Complexes Displaying Either Single Molecule Magnet or Luminescence—Direct Magnetic and Photo-Physical Correlations in the Ytterbium Analogue. *Inorg. Chem.* **2013**, *52*, 5978−5990. (d) Han, T.; Shi, W.; Zhang, X. P.; Li, L. L.; Cheng, P. A Family of Binuclear Dysprosium(III) Radical Compounds with Magnetic Relaxation in ON and OFF States. *Inorg. Chem.* **2012**, *51*, 13009−13016. (e) Eliseeva, S. V.; Ryazanov, M.; Gumy, F.; Troyanov, S. I.; Lepnev, L. S.; Bünzli, J. C. G.; Kuzmina, N. P. Dimeric Complexes of Lanthanide(III) Hexafluoroacetylacetonates with 4-Cyanopyridine N-Oxide: Synthesis, Crystal Structure, Magnetic and Photoluminescent Properties. *Eur. J. Inorg. Chem.* **2006**, *2006*, 4809−4820. (f) Murashima, K.; Karasawa, S.; Yoza, K.; Inagaki, Y.; Koga, N. 3- and 4 ([α]-diazobenzyl)pyridine-N-oxides as photoresponsive magnetic couplers for 2p-4f heterospin systems: formation of carbene-Tb^{III} and carbene-Dy^{III} single-molecule magnets. *Dalton Trans.* **2016**, *45*, 7067−7077. (g) Pointillart, F.; Le Guennic, B.; Maury, O.; Golhen, S.; Cador, O.; Ouahab, L. Lanthanide Dinuclear Complexes Involving Tetrathiafulvalene-3-pyridine-N-oxide Ligand: Semiconductor Radical Salt, Magnetic, and Photophysical Studies. *Inorg. Chem.* **2013**, *52*, 1398−1408. (h) Pointillart, F.; Le Gal, Y.; Golhen, S.; Cador, O.; Ouahab, L. Single-Molecule Magnet Behaviour in a Tetrathiafulvalene-Based Electroactive Antiferromagnetically Coupled Dinuclear Dysprosium(III) Complex. *Chem. - Eur. J.* **2011**, *17*, 10397−10404. (i) Kiefl, E.; Mannini, M.; Bernot, K.; Yi, X.; Amato, A.; Leviant, T.; Magnani, A.; Prokscha, T.; Suter, A.; Sessoli, R.; Salman, Z. Robust Magnetic Properties of a Sublimable Single-Molecule Magnet. *ACS Nano* **2016**, *10*, 5663−5669. (j) Zhu, W.; Xiong, X.; Gao, C.; Li, S.; Zhang, Y.; Wang, J.; Zhang, C.; Powell, A. K.; Gao, S. A family of one-dimensional lanthanide complexes bridged by two distinct carboxylate ligands with the Dy analogue displaying magnetic relaxation behaviour. *Dalton Trans.* **2017**, *46*, 14114−14121.
(10) (a) Wang, Y.-L.; Ma, Y.; Yang, X.; Tang, J.; Cheng, P.; Wang, Q.-L.; Li, L.-C.; Liao, D.-Z. Syntheses, Structures, and Magnetic and Luminescence Properties of a New DyIII-Based Single-Ion Magnet. *Inorg. Chem.* **2013**, *52*, 7380−7386. (b) Chen, G.-J.; Gao, C.-Y.; Tian, J.-L.; Tang, J.; Gu, W.; Liu, X.; Yan, S.-P.; Liao, D.-Z.; Cheng, P. Coordination-perturbed single-molecule magnet behaviour of mononuclear dysprosium complexes. *Dalton Trans.* **2011**, *40*, 5579−5583. (c) Chen, G.-J.; Guo, Y.-N.; Tian, J.-L.; Tang, J.; Gu, W.; Liu, X.; Yan, S.-P.; Cheng, P.; Liao, D.-Z. Enhancing Anisotropy Barriers of Dysprosium(III) Single-Ion Magnets. *Chem. - Eur. J.* **2012**, *18*, 2484−2487. (d) Cen, P.-P.; Zhang, S.; Liu, X.-Y.; Song, W.-M.; Zhang, Y.-Q.; Xie, G.; Chen, S.-P. Electrostatic Potential Determined Magnetic Dynamics Observed in Two Mononuclear β-Diketone Dysprosium(III) Single-Molecule Magnets. *Inorg. Chem.* **2017**, *56*, 3644−3656. (e) Tong, Y.-Z.; Gao, C.; Wang, Q.-L.; Wang, B.-W.; Gao, S.; Cheng, P.; Liao, D.-Z. Two mononuclear single molecule magnets derived from dysprosium(III) and tmphen (tmphen = 3,4,7,8-tetramethyl-1,10-phenanthroline). *Dalton Trans.* **2015**, *44*, 9020−9026. (f) Sun, W.-B.; Yan, B.; Jia, L.-H.; Wang, B.-W.; Yang, Q.; Cheng, X.; Li, H.-F.; Chen, P.; Wang, Z.-M.; Gao, S. Dinuclear dysprosium SMMs bridged by a neutral bipyrimidine ligand: two crystal systems that depend on different lattice solvents lead to a distinct slow relaxation behavior. *Dalton Trans.* **2016**, *45*, 8790−8794. (g) Yu, W.; Schramm, F.; Pineda, E. M.; Lan, Y.; Fuhr, O.; Chen, J.; Isshiki, H.; Wernsdorfer, W.; Wulfhekel, W.; Ruben, M. Single-molecule magnet behavior in 2,2'-bipyrimidine-bridgeddilanthanide complexes. *Beilstein J. Nanotechnol.* **2016**, *7*, 126−137.
(11) Corey, E. J.; Borror, A. L.; Foglia, T. Transformations in the 1,10-Phenanthroline Series. *J. Org. Chem.* **1965**, *30*, 288−290.
(12) Rodríguez-Dieguez, A.; Kivekas, R.; Sakiyama, H.; Debdoubi, A.; Colacio, E. A novel 3D cyano-bridged mixed-valence CoII/CoIII canted antiferromagnet constructed from defective cubanes. Synthesis, X-ray structure and magnetic properties. *Dalton Trans.* **2007**, *0*, 2145−2149.
(13) Sheldrick, G. M. A short history of SHELX. *Acta Crystallogr., Sect. A: Found. Crystallogr.* **2008**, *64*, 112−122.
(14) Dolomanov, O. V.; Bourhis, L. J.; Gildea, R. J.; Howard, J. A. K.; Puschmann, H. OLEX2: A complete structure solution, refinement and analysis program. *J. Appl. Crystallogr.* **2009**, *42*, 339−341.
(15) Nojiri, H.; Choi, K.-Y.; Kitamura, N. Manipulation of the quantum tunneling of nanomagnets by using time-dependent high magnetic fields. *J. Magn. Magn. Mater.* **2007**, *310*, 1468−1472.
(16) (a) Aquilante, F.; Autschbach, J.; Carlson, R. K.; Chibotaru, L. F.; Delcey, M. G.; De Vico, L.; Fdez. Galván, I.; Ferré, N.; Frutos, L. M.; Gagliardi, L.; Garavelli, M.; Giussani, A.; Hoyer, C. E.; Li Manni, G.; Lischka, H.; Ma, D.; Malmqvist, P. Å.; Müller, T.; Nenov, A.; Olivucci, M.; Pedersen, T. B.; Peng, D.; Plasser, F.; Pritchard, B.; Reiher, M.; Rivalta, I.; Schapiro, I.; Segarra-Martí, J.; Stenrup, M.; Truhlar, D. G.; Ungur, L.; Valentini, A.; Vancoillie, S.; Veryazov, V.; Vysotskiy, V. P.; Weingart, O.; Zapata, F.; Lindh, R. Molcas 8: New capabilities for multiconfigurational quantum chemical calculations across the periodic table. *J. Comput. Chem.* **2016**, *37*, 506−541. (b) Aquilante, F.; De Vico, L.; Ferre, N.; Ghigo, G.; Malmqvist, P. A.; Neogrady, P.; Pedersen, T. B.; Pitonak, M.; Reiher, M.; Roos, B. O.; Serrano-Andres, L.; Urban, M.; Veryazov, V.; Lindh, R. MOLCAS 7: The Next Generation. *J. Comput. Chem.* **2010**, *31*, 224−247. (c) Duncan, J. A. Molcas 7.2. *J. Am. Chem. Soc.* **2009**, *131*, 2416−2416. (d) Veryazov, V.; Widmark, P. O.; Serrano-Andres, L.; Lindh, R.; Roos, B. O. 2MOLCAS as a development platform for quantum chemistry software. *Int. J. Quantum Chem.* **2004**, *100*, 626−635. (e) Karlstrom, G.; Lindh, R.; Malmqvist, P. A.; Roos, B. O.; Ryde, U.; Veryazov, V.; Widmark, P. O.; Cossi, M.; Schimmelpfennig, B.; Neogrady, P.; Seijo, L. MOLCAS: a program package for computational chemistry. *Comput. Mater. Sci.* **2003**, *28*, 222−239.
(17) Chibotaru, L. F.; Ungur, L. Ab initio calculation of anisotropic magnetic properties of complexes. I. Unique definition of pseudospin Hamiltonians and their derivation. *J. Chem. Phys.* **2012**, *137*, 064112-1−064112-22.
(18) (a) Langley, S. K.; Ungur, L.; Chilton, N. F.; Moubaraki, B.; Chibotaru, L. F.; Murray, K. S. Single-Molecule Magnetism in a Family of {CoIII2DyIII2} Butterfly Complexes: Effects of Ligand Replacement on the Dynamics of Magnetic Relaxation. *Inorg. Chem.* **2014**, *53*, 4303−4315. (b) Habib, F.; Luca, O. R.; Vieru, V.; Shiddiq, M.; Korobkov, I.; Gorelsky, S. I.; Takase, M. K.; Chibotaru, L. F.; Hill, S.; Crabtree, R. H.; Murugesu, M. Influence of the Ligand Field on Slow Magnetization Relaxation versus Spin Crossover in Mononuclear Cobalt Complexes. *Angew. Chem., Int. Ed.* **2013**, *52*, 11290−11293.
(19) Roos, B. O.; Lindh, R.; Malmqvist, P. A.; Veryazov, V.; Widmark, P. O.; Borin, A. C. New Relativistic Atomic Natural Orbital Basis Sets for Lanthanide Atoms with Applications to the Ce Diatom and LuF_3. *J. Phys. Chem. A* **2008**, *112*, 11431−11435.
(20) Koch, H.; Sánchez de Merás, A.; Pedersen, T. B. Reduced scaling in electronic structure calculations using Cholesky decompositions. *J. Chem. Phys.* **2003**, *118*, 9481−9484.
(21) Ungur, L.; Chibotaru, L. F. *POLY_ANISO program*; KU Leuven: Leuven, Belgium, 2007.
(22) (a) Ungur, L.; Thewissen, M.; Costes, J.-P.; Wernsdorfer, W.; Chibotaru, L. F. Interplay of Strongly Anisotropic Metal Ions in Magnetic Blocking of Complexes. *Inorg. Chem.* **2013**, *52*, 6328−6337. (b) Feltham, H. L. C.; Lan, Y.; Klöwer, F.; Ungur, L.; Chibotaru, L. F.; Powell, A. K.; Brooker, S. A Non-sandwiched Macrocyclic Monolanthanide Single-Molecule Magnet: The Key Role of Axiality. *Chem. - Eur. J.* **2011**, *17*, 4362−4365. (c) Ungur, L.; Chibotaru, L. F. Magnetic anisotropy in the excited states of low symmetry lanthanide complexes. *Phys. Chem. Chem. Phys.* **2011**, *13*, 20086−20090.

DOI: 10.1021/acs.inorgchem.8b00427
Inorg. Chem. 2018, 57, 6362−6375

(23) Llunell, M.; Casanova, D.; Cirera, J.; Bofill, J. M.; Alemany, P.; Alvarez, S.; Pinsky, M.; Avnir, D. *SHAPE v1.1b program*; Barcelona, Spain, 2005.
(24) Bi, Y.; Guo, Y. − N.; Zhao, L.; Guo, Y.; Lin, S. − Y.; Jiang, S. − D.; Tang, J.; Wang, B. − W.; Gao, S. Capping Ligand Perturbed Slow Magnetic Relaxation in Dysprosium Single-Ion Magnets. *Chem. - Eur. J.* **2011**, *17*, 12476−12481.
(25) Chilton, N. F. *CCFIT program*; The Chilton Group: Manchester, U.K., 2014; http://www.nfchilton.com/software.html.
(26) (a) Feltham, H. L. C.; Lan, Y.; Klöwer, F.; Ungur, L.; Chibotaru, L. F.; Powell, A. K.; Brooker, S. A Non-sandwiched Macrocyclic Monolanthanide Single-Molecule Magnet: The Key Role of Axiality. *Chem. - Eur. J.* **2011**, *17*, 4362−4365. (b) Costes, J. P.; Titos-Padilla, S.; Oyarzabal, I.; Gupta, T.; Duhayon, C.; Rajaraman, G.; Colacio, E. Analysis of the Role of Peripheral Ligands Coordinated to ZnII in Enhancing the Energy Barrier in Luminescent Linear Trinuclear Zn-Dy-Zn Single-Molecule Magnets. *Chem. - Eur. J.* **2015**, *21*, 15785−15796.
(27) (a) Rinehart, J. D.; Long, J. R. Exploiting single-ion anisotropy in the design of f-element single-molecule magnets. *Chem. Sci.* **2011**, *2*, 2078−2085. (b) Kajiwara, T.; Nakano, M. K.; Takahashi, S.; Takaishi, S.; Yamashita, M. Structural Design of Easy-Axis Magnetic Anisotropy and Determination of Anisotropic Parameters of LnIII−CuII Single-Molecule Magnets. *Chem. - Eur. J.* **2011**, *17*, 196−205. (c) Watanabe, A.; Yamashita, A.; Nakano, M.; Yamamura, T.; Kajiwara, T. Multi-Path Magnetic Relaxation of Mono-Dysprosium(III) Single-Molecule Magnet with Extremely High Barrier. *Chem. - Eur. J.* **2011**, *17*, 7428−7432.
(28) Abragam, A.; Bleaney, B. *Electron Paramagnetic Resonance of Transition Ions*; Clarendon Press: Oxford, U.K., 1970.
(29) Marx, R.; Moro, F.; Dörfel, M.; Ungur, L.; Waters, M.; Jiang, S. D.; Orlita, M.; Taylor, J.; Frey, W.; van Slageren, J.; Chibotaru, L. F. Spectroscopic determination of crystal field splittings in lanthanide double deckers. *Chem. Sci.* **2014**, *5*, 3287−3293.
(30) Gómez-Coca, S.; Aravena, D.; Morales, R.; Ruiz, E. Large magnetic anisotropy in mononuclear metal complexes. *Coord. Chem. Rev.* **2015**, *289-290*, 379−392.
(31) Ungur, L.; Thewissen, M.; Costes, J. P.; Wernsdorfer, W.; Chibotaru, L. F. Interplay of strongly anisotropic metal ions in magnetic blocking of complexes. *Inorg. Chem.* **2013**, *52*, 6328−6337.
(32) (a) Venugopal, A.; Tuna, F.; Spaniol, T. P.; Ungur, L.; Chibotaru, L. F.; Okuda, J.; Layfield, R. A. A hydride-ligated dysprosium single-molecule magnet. *Chem. Commun.* **2013**, *49*, 901−903. (b) Habib, F.; Brunet, G.; Vieru, V.; Korobkov, I.; Chibotaru, L. F.; Murugesu, M. Significant Enhancement of Energy Barriers in Dinuclear Dysprosium Single-Molecule Magnets Through Electron-Withdrawing Effects. *J. Am. Chem. Soc.* **2013**, *135*, 13242−13245. (c) Zhang, K.; Yuan, C.; Guo, F.-S.; Zhang, Y.-Q.; Wang, Y.-Y. Fine-tuning terminal solvent ligands to rationally enhance the energy barrier in dinuclear dysprosium single-molecule magnets. *Dalton Trans.* **2017**, *46*, 186−192. (d) Tuna, F.; Smith, C. A.; Bodensteiner, M.; Ungur, L.; Chibotaru, L. F.; McInnes, E. J. L.; Winpenny, R. E. P.; Collison, D.; Layfield, R. A. A High Anisotropy Barrier in a Sulfur-Bridged Organodysprosium Single-Molecule Magnet. *Angew. Chem., Int. Ed.* **2012**, *51*, 6976−6980. (e) Guo, Y.-N.; Xu, G.-F.; Wernsdorfer, W.; Ungur, L.; Guo, Y.; Tang, J.; Zhang, H.-J.; Chibotaru, L. F.; Powell, A. K. Strong Axiality and Ising Exchange Interaction Suppress Zero-Field Tunneling of Magnetization of an Asymmetric Dy2 Single-Molecule Magnet. *J. Am. Chem. Soc.* **2011**, *133*, 11948−11951.
(33) Upadhyay, A.; Singh, S. K.; Das, C.; Mondol, R.; Langley, S. K.; Murray, K. S.; Rajaraman, G.; Shanmugam, M. Enhancing the effective energy barrier of a Dy(III) SMM using a bridged diamagnetic Zn(II) ion. *Chem. Commun.* **2014**, *50*, 8838−8841.
(34) Liu, J.-L.; Chen, Y.-C.; Zheng, Y.-Z.; Lin, W.-Q.; Ungur, L.; Wernsdorfer, W.; Chibotaru, L. F.; Tong, M.-L. Switching the anisotropy barrier of a single-ion magnet by symmetry change from quasi-D_{5h} to quasi-O_h. *Chem. Sci.* **2013**, *4*, 3310−3316.
(35) Oyarzabal, I.; Rodríguez-Diéguez, A.; Barquín, M.; Seco, J. M.; Colacio, E. The effect of the disposition of coordinated oxygen atoms on the magnitude of the energy barrier for magnetization reversal in a family of linear trinuclear Zn−Dy−Zn complexes with a square-antiprism DyO_8 coordination sphere. *Dalton Trans.* **2017**, *46*, 4278−4286.
(36) Saito, K.; Miyashita, S. Magnetic Foehn Effect in Adiabatic Transition. *J. Phys. Soc. Jpn.* **2001**, *70*, 3385−3390.

DOI: 10.1021/acs.inorgchem.8b00427
Inorg. Chem. 2018, 57, 6362−6375